Relative geomagnetic paleointensity of the Brunhes Chron and the Matuyama-Brunhes precursor as recorded in sediment core from Wilkes Land Basin (Antarctica)

Patrizia Macrì, Leonardo Sagnotti, Jaume Dinarès-Turell, Andrea Caburlotto

Accepted Manuscript

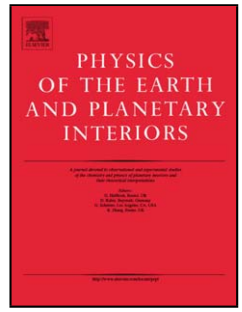

Title: Relative geomagnetic paleointensity of the Brunhes Chron and the Matuyama-Brunhes precursor as recorded in sediment core from Wilkes Land Basin (Antarctica)

Authors: Patrizia Macrì, Leonardo Sagnotti, Jaume Dinarès-Turell, Andrea Caburlotto

PII: S0031-9201(09)00241-6
DOI: doi:10.1016/j.pepi.2009.12.002
Reference: PEPI 5230

To appear in: *Physics of the Earth and Planetary Interiors*

Received date: 24-7-2009
Revised date: 4-12-2009
Accepted date: 7-12-2009

Relative geomagnetic paleointensity of the Brunhes Chron and the Matuyama-Brunhes precursor as recorded in sediment core from Wilkes Land Basin (Antarctica)

Patrizia Macrì[1], Leonardo Sagnotti[1], Jaume Dinarès-Turell[1] and Andrea Caburlotto[2]

[1] Istituto Nazionale di Geofisica e Vulcanologia, Via di Vigna Murata 605, 00143 Roma, Italy. (Tel: +39 0651860700; fax: +39 0651860397; e-mail: macri@ingv.it).

[2] Istituto Nazionale di Oceanografia e Geofisica Sperimentale, Borgo Grotta Gigante 42/c, 34010 Sgonico, Trieste, Italy

Abstract

Paleomagnetic and rock magnetic investigation was performed on the 35-m long MD03-2595 CADO (Coring Adélie Diatom Oozes) piston core recovered on the continental rise of the Wilkes Land Basin (East Antarctica). Analysis of the Characteristic Remanent Magnetization (ChRM) inclination record indicates a normal magnetic polarity for the uppermost 34 m of the sequence and a distinctive abrupt polarity change at the bottom of the core. This polarity change, which spans a 27 cm thick stratigraphic interval, represents a detailed record of the Matuyama-Brunhes (M-B) transition and it is preceded by a sharp oscillation in paleomagnetic directions that may correlate to the M-B precursor event. Paleomagnetic measurements enable reconstruction of geomagnetic relative paleointensity (RPI) variations, and a high-resolution age model was established by correlating the CADO RPI curve to the available global reference RPI stack, indicating that the studied sequence reaches back to ca 800 ka with an average sedimentation rate of 4.4 cm/ka. Orbital periodicities (100 ka and 41 ka) were found in the ChRM inclination record, and a significant coherence of ChRM inclination and RPI record around 100 ka suggests that long-term geomagnetic secular variation in inclination is controlled by changes in the relative strength of the geocentric axial dipole and persistent non-dipole components. Moreover, even if the relatively homogeneous rock magnetic parameters and

lithofacies throughout the recovered sequence indicates a substantial stability of the East Antarctic Ice Sheet during the middle and late Pleistocene, influence of the 100 ka and 41 ka orbital periodicities has been detected in some rock magnetic parameters, indicating subtle variations in the concentration and grain-size of the magnetic minerals linked to orbital forcing of the global climate.

Keywords**:** paleomagnetism, relative paleointensity, Brunhes Chron, Matuyama-Brunhes precursor, Antarctica.

1. Introduction

Pleistocene sedimentary sequences from peri-Antarctic margins have great potential for studies of paleoenvironmental changes and past geomagnetic field behavior at high latitudes: the Antarctic continental rises are very sensitive to past environmental and climatic changes, and their marine sedimentary sequences may preserve detailed information about past climatic variations. Well resolved paleomagnetic data from high latitudes are also critically important for global reconstruction of past geomagnetic field behavior and can provide critical constraints for geodynamo modelling.

The QUASAR (QUAternary Sedimentary processes on the east Antarctic continental Rise) project of the Italian Programma Nazionale Ricerche in Antartide-PNRA, focus on a multiproxy analysis of the MD03-2595 CADO (Coring Adélie Diatom Oozes) piston core recovered on the continental rise of the Wilkes Land Basin (WLB) which consists of a continuous fine-grained sedimentary sequence with a high chronostratigraphic potential. The QUASAR project aims to reconstruct sedimentary processes offshore of the east Antarctic continental margin and to infer climatic fluctuations of the continental East Antarctic Ice Sheet.

We present a paleomagnetic and rock magnetic study of the 35-m long CADO core, with the reconstruction of geomagnetic relative paleointensity (RPI) and Characteristic Remanent Magnetization (ChRM) direction stratigraphic records. The obtained paleomagnetic data allow to establish of a high-resolution age model and to quantify the sedimentation rate for the recovered sequence. This is particularly valuable because the corrosive character of Antarctic deep waters with respect to carbonate implies that peri-Antarctic sediments are commonly deprived of age constraints derived from micropaleontology or stable isotope stratigraphy.

The MD03-2595 CADO core is located just outside the inner core tangent cylinder, an imaginary cylinder parallel to the Earth's spin axis that circumscribes the equator of the inner core and intersects the surface of the Earth in the polar regions at a latitude of ca 69.6° in both hemispheres. Different models indicate that geodynamo action occurs mainly by polar vortices within the tangent cylinder [e.g., Glatzmaier and Roberts, 1995a; Aurnou et al., 2003] or by differential rotation outside the tangent cylinder [e.g., Kuang and Bloxham, 1997]. Glatzmaier and Roberts [1995b] showed that there were strong toroidal fields and differential rotation within the tangent cylinder, with high density of magnetic flux patches that strengthen the non-dipolar component of the geomagnetic field over the polar regions. This might cause a larger dynamics, complexity and variability of the geomagnetic field within the tangent cylinder with respect to the intermediate and low latitudes. The available paleomagnetic study of several cores from the Arctic region indicates that the magnetic field has been strongly variable during at least the last 300 ka [e.g. Nowaczyk and Antonow, 1997; Nowaczyk and Frederichs, 1999], with geomagnetic excursions more frequent and of longer duration than elsewhere. In this context, only additional studies on sedimentary sequences from southern and northern high latitudes can provide the necessary experimental evidence to understand past geomagnetic variability within the polar regions, inside or close to the surface projection of the tangent cylinder.

In this context, since there are only few relative paleointensity determinations from high southern latitudes, along the peri-Antarctic margins [e.g. Brachfeld et al., 2000; 2003; Sagnotti et al., 2001; Macrì et al., 2005; 2006], the reconstruction of a high-resolution paleomagnetic record from the CADO sediments represents a valuable input for understanding geomagnetic field dynamics in the Antarctic region during the past few kyrs.

2 Geological setting and lithostratigraphy

The MD03-2595 CADO core was recovered during the MD130 cruise of the R/V "Marion Dufresne II" from the continental rise of the WLB on a sediment wave field in front of the Mertz Glacier (Lat. 64° 54.04 S, Long. 144° 46.37 E) (Fig. 1A). The depositional system of the WLB was formerly investigated by the joint Australian and Italian WEGA (WilkEs land GlAcial history) Project, with about 600 km of multichannel seismic reflection and 3.5 kHz acoustic profiles and 11 piston cores triggered [see Brancolini and Harris, 2000]. The morphology of this area is characterized by several submarine canyons incising the slope, and a ridge-channel system perpendicular to the continental margin that originated from the interplay of turbidites and bottom currents [Escutia et al., 1997; Rebesco et al., 1997; Busetti et al., 2003]. The 35-m long CADO core was collected along the transect "Line W39" (Fig. 1A) crossing the depositional flank of the sediment ridge B and the Buffon Canyon (Fig. 1B), and it recovered a continuous sedimentary sequence characterized by a higher chronostratigraphic potential with respect to the already studied and relatively short WEGA cores (each ca 4 meter long) collected in the adjacent area (see Fig. 1A). The sedimentary sequence consists of very fine-grained terrigenous sediments including intervals of massive homogeneous mud, with some sparse fine-grained ice rafted debris (IRD), alternated to laminated mud intervals interpreted as the result of traction currents and\or distal turbidities [Escutia et al., 1997; Busetti et al., 2003; Caburlotto, 2003]. The massive mud facies appears bioturbated, particularly in the first 6 m at the top of the core, and are characterized by a relatively higher content of organic matter and well preserved open-ocean diatoms. The laminated intervals are composed of mm- to cm-thick muddy and silty layers with lack of bioturbation and general lower content of organic matter.

3. Sampling and methods

In December 2004, 1.5 m long u-channels were sampled from the 24 archive sections of the MD03-2595 core at the core repository of the Antarctic Climate and Ecosystems Cooperative Research Centre-CRC in Canberra, Australia. Because of empty sections, u-channel samples were not collected for 640-660 cm, 790-820 cm, 1007-1050 cm, 1209-1221 cm, and 1450-1519 cm depth intervals of core.

The u-channels were then measured in a magnetically shielded paleomagnetic laboratory at the Istituto Nazionale di Geofisica e Vulcanologia, Rome, using an automated pass through 2-G Enterprises DC SQUID cryogenic magnetometer system with a 4.5 cm pass through diameter access and an in-line Bartington instrument MS2C susceptibility loop sensor, a set of three orthogonal alternating field (AF) demagnetizing coils with optional anhysteretic remanent magnetization (ARM) capabilities and an isothermal remanent magnetization (IRM) pulse magnetizer. High-resolution (1-cm spacing) records of natural remanent magnetization (NRM), ARM and low-field volume specific magnetic susceptibility (κ) were obtained for all u-channels from the MD03-2595 core.

The raw magnetic moment data measured by the three orthogonal SQUID sensors of the cryogenic magnetometer were corrected, directly by the measuring software, taking into account the different areas under the SQUID response curves. This correction compensates for the effects of the negative regions on the edge of the response functions for the transverse axes and for the broader width of the response function along the long axis of the u-channel. It therefore ensures that the data are free from artefacts that may result from an inadequate consideration of the different widths and shapes of the response functions for the three SQUID pick-up coils, which could result in fictitious inclination shallowing (or steepening) of the paleomagnetic data [see Roberts, 2006]. Moreover, we took particular care in avoiding artefacts eventually due to deformation effects introduced during sampling, which could result in remanence deflections. We adopted a conservative approach in this study, disregarding the paleomagnetic data for ~5cm at both ends of each u-channel and stratigraphic gap.

After measuring κ, the NRM was progressively subjected to alternating field (AF) demagnetization in nine steps up to a maximum peak field of 100 mT. Then, an ARM was imparted by translating the u-channels at a speed of 10 cm/s in a constant symmetric AF of 100 mT with a superimposed direct current (DC) bias field of 0.1 mT, which was subsequently stepwise demagnetized using the same sequence of AF steps applied to the NRM. An IRM was then imparted in a steady DC field of 0.9 T. However the intensity of the IRM exceeded the dynamic range of the SQUIDs, so we do not report these data below. In order to investigate the magnetic mineralogy of the sediments, specific rock magnetic investigations were also performed on eight representative powder samples. Magnetic susceptibility variations in heating-cooling cycles from room temperature up to 700°C were obtained using a Kappabridge KLY-3 AGICO magnetic susceptibility meter, coupled with a CS3 furnace. Hysteresis properties, including coercive force (B_C), saturation remanent magnetization (M_{RS}) and saturation magnetization (M_S) were measured on a MicroMag alternating gradient magnetometer (AGM model 2900, Princeton Measurements Corporation) with a maximum applied field of 1 T. The acquisition of an IRM, and subsequent back-field remagnetization, both in a succession of fields up to 1 T, was obtained with the same AGM instrument. The remanent coercive force (B_{CR}) was computed from the back-field remagnetization curves.

4. Results

4.1. Paleomagnetism

Demagnetization diagrams (Fig. 2) indicate stable paleomagnetic behavior throughout most of the core, with the data aligned along linear demagnetization paths toward the origin, after removal of a viscous low coercivity remanence component at 10-20 mT. The characteristic remanent magnetization (ChRM) was computed by principal component analysis on the individual linear demagnetization paths [Kirschvink, 1980], measured at 1 cm spacing, and was generally isolated in the 20-80 mT, or rarely 40-80 mT, step intervals. The ChRM was not identified in a few short intervals, that are characterized by unstable paleomagnetic behavior, and for the depth interval 1955-2095 cm, because a technical trouble occurred during demagnetization steps higher than 20mT for u-channel 14. Fig. 3 shows the downcore stratigraphic trends of the ChRM declination and inclination, the maximum angular deviation (MAD) and the RPI curves NRM_{20mT}/κ and NRM_{20mT}/ARM_{20mT}. The high latitude of the study site guarantees that the ChRM inclination is representative enough of the paleomagnetic vectors, and can provide unambiguous identification of the paleomagnetic polarity. The ChRM inclination trend shows that the core is mostly of normal polarity. A distinctive abrupt polarity change is recorded at the bottom of the core, across ca 27 cm of section, with the 0° inclination mid-point positioned at a depth of ca 3400 cm. About 45 cm below the polarity transition, another sharp inclination swing, spanning ca 12 cm of section, is recorded: the inclinations pass again through the horizontal, approach full normal polarity (-73°), and then quickly progress to shallow values and finally return back to the reverse polarity mean values. With regards to the ChRM declination, we point out that even if the absolute azimuthal orientation is not granted for each u-channel and relative azimuthal displacements are possible at each u-channel and stratigraphic break, it generally consistently oscillates around 360°. A few sharp, and stratigraphically limited, ChRM declination oscillations mostly correspond to intervals of nearly vertical ChRM or to the polarity transition. MAD angles are usually less than 2° along the core, indicating that the ChRM directions are generally very well defined; higher values (MAD up to 15°) were obtained for a few intervals at the bottom of the core in correspondence to the polarity transition (Fig. 3). The RPI records, computed by normalizing the NRM_{20mT} by κ and ARM_{20mT}, show a similar pattern supporting a general coherency between the two normalization procedures. RPI records will be discussed in closer detail in section 4.3.

4.2 Rock magnetism

In Fig. 4 we show the downcore stratigraphic trends of the main rock magnetic parameters measured for the MD03-2595 CADO core. Oscillations of the magnetic susceptibility κ and of the ARM_{0mT} intensities throughout the core are limited, with values comprised within the same order of magnitude, which is one of the requisites to obtain reliable RPI estimates (e.g., Tauxe, 1993). In particular, κ fluctuates around a mean value of 35 x 10^{-5} SI (with a full range of variability from ca 5 x 10^{-5} SI to 60 x 10^{-5} SI), with few sharp peaks corresponding to sparse pebbles or mm thick silty layers. ARM_{0mT} mostly oscillates around 2 x 10^{-1} A/m (with a full range of variability from 0.05 to 5 x 10^{-1} A/m). As a result of the limited variation of both κ and ARM_{0mT}, the ARM_{0mT}/κ ratio is also rather constant, with values fluctuating between 0.5 and 1.5 x 10^{3} A/m. The median destructive field of the NRM (MDF_{NRM}) is generally comprised between 10 and 40 mT; several swings to lower and higher MDF_{NRM} values (from 5 mT to 50 mT, respectively) are evident in the bottom part of the core (last 3-4 m) where the intensity of the NRM is lower. The MDF_{ARM} values show a substantial uniformity as well, with a mean value of ca 28 mT. The ranges of variability for all the rock magnetic parameters are very similar to the those observed in the nearby WEGA cores [Macrì et al., 2005].

In order to perform rock magnetic analysis, 8 sub-samples were directly picked from the u-channels at different selected levels corresponding to high/low MDF_{NRM} or ARM_{0mT}/κ values (Fig. 4). All thermomagnetic curves (Fig. 5A, B, C) show an abrupt decrease of the magnetic susceptibility value at a temperature of 550°-580°C, corresponding to the Curie temperature of magnetite (Fe_3O_4). Several samples are also characterized by a peak at ca 280°C followed by a distinctive decrease between 280°C and 430°C (fig 5A, B), that may be due to the thermally induced conversion of maghaemite (γ-Fe_2O_3) to haematite (α-Fe_2O_3) [Stacey and Banerjee, 1974]. The presence of hematite is indicated by the decreasing trend of the heating curves above 580°C, which is observed in some samples. A thermally induced production of newly formed magnetite is indicate by the cooling curves which are always well above the heating curves (e.g.

fig 5A). Hysteresis loops from the same samples generally indicate a coercivity (B_c) of ca 20 mT (Fig. 6A), only two samples are characterized by lower coercivity (B_c of ca 10 mT) (Fig. 6B). The hysteresis ratios mostly fall in a restricted region of the "Day plot" [Day et al., 1977], typical of pseudo-single domain (PSD) magnetite grains (Fig. 6C). The κARM vs. κ plot can be used to infer grain size variations of ferrimagnetic particles [e.g. King et al., 1983], even if we recognize that, in practice, it cannot be rigorously applied to determine the actual grain size of magnetite particles because the ARM intensity varies significantly depending on the experimental procedures, not yet fully standardized between individual laboratory [see Sagnotti et al., 2003], and because magnetostatic interaction may affect the efficiency of ARM acquisition [Sugiura, 1979; Yamazaki and Ioka, 1997]. However, the κARM vs. κ plot indicates a substantial uniformity in the overall magnetic mineral grain size of the sediments (Fig. 6D), with few, but pronounced, departures from the main cluster of the data corresponding to distinctive peaks in the magnetic susceptibility linked to rare pebbles or silty layers (i.e. 30-33 cm, 1792-1795 cm, 2826-2829 cm, 2934-2937 cm and 3181-3193 cm depth intervals, see Fig. 3). These intervals, which provided rock magnetic data out of the typical range of variability, were not taken into account for the reconstruction of the RPI records.

Further rock magnetic measurements are available on 70 discrete samples selected from the WEGA cores [see Macrì et al., 2005], which show hysteresis parameters and thermomagnetic curves that are very similar to those measured for the CADO samples.

We conclude that all the rock magnetic parameters of the WEGA and the CADO cores indicate that these sediments share the same magnetic carriers, which consists of low-coercivity minerals, most likely represented by a mixture of PSD magnetite and maghemite grains.

4.3 Relative paleointensity and age model

As the CADO core shows a well defined ChRM and fulfils the basic requirements of a substantial uniformity in lithology and in concentration, composition and grain size of the magnetic minerals [King et al., 1983; Meynadier et al., 1992; Tauxe, 1993; Valet and Meynadier, 1998], we used the obtained paleomagnetic and rock magnetic data to reconstruct variation in relative paleointensity of the geomagnetic field. RPI curves were computed by normalizing the NRM demagnetized at 20 mT with different concentration-dependent rock magnetic parameters (NRM_{20mT}/κ and NRM_{20mT}/ARM_{20mT}) (see Fig. 3). All the data far from the uniformity criteria, and that could affect the normalized intensities, were not included in the reconstruction of the RPI records. The two RPI curves generally match closely, showing the same stratigraphic patterns throughout the core and only different amplitude in some levels.

We considered the NRM_{20mT}/κ record as the best RPI proxy (as discussed below) and then we correlated it to the available global RPI stack SINT-800 of Guyodo & Valet [1999] (Fig. 7A). Ages from the dated reference curve were transferred to the CADO RPI record on the basis of visual correlation of the main paleointensity features using the Analyseries 1.2 software of Paillard et al. [1996], which allows adjustment and dating between selected pairs of depth and age tie points of two numerical series. Result of correlation indicates that the CADO core extends back to about 800 ka across the Matuyama-Brunhes (M-B) polarity transition (Fig. 7B).

The reconstructed average sediment accumulation rate ranges from 1.6 to 8.6 cm/ka (as calculated from the ages assigned at the individual tie-points; see the step-like line in Fig. 7C). The mean sedimentation rate for the entire core is 4.4 cm/ka, which is compatible with its position within the WLB, close to the depositional flank of the sediment ridge B. By comparison, the average sedimentation rates for six short cores collected in an adjacent area varied between 19 cm/ka for core PC19 along the WEGA channel and 0.6 cm/ka for core PC20 which was recovered from a ridge crest [Macrì et al., 2005].

The CADO RPI record was also compared with the PISO-1500 global RPI stack recently published by Channell et al. [2009] and with other southern high latitude records compiled by Tauxe and Yamazaki [2007] and available from the database of the Magnetics Information

Consortium (MagIC) website (Fig. 8). This comparison indicates that the major RPI lows may be considered global in nature and serve as a target for age control.

In order to confirm the efficiency of the RPI normalization procedure, we tested whether the normalized records are coherent with respect to each other and with respect to the normalization parameters, using the coherence function (Fig. 9). Times series were at first prepared by removing any linear trend using a linear function (integration method), after that the spectral analysis was performed using the software package Analyseries 1.2 [Paillard et al., 1996] with the Blackman-Tukey method, a Bartlett window and a band-width of ca 0.006 kyr^{-1}.

The coherence function analysis suggests that the normalized intensity curves are coherent with each other over most of the relevant frequency range, but they are generally not coherent with the normalization parameters, especially for NRM_{20mT}/κ series (showing significant coherence above the 95% confidence level only in frequencies from 0.005 to 0.011, roughly around the 100 kyr eccentricity cycle) (Fig. 9A). A coherence extending also to higher and lower frequencies was obtained for the NRM_{20mT}/ARM_{20mT} and ARM_{20mT} parameters. Usually the efficiency of ARM acquisition may be decreased by magnetostatic interaction between SD grains [Sugiura, 1979]. This effect could bring to an erroneous evaluation of the magnetizability of the sediment when using ARM as the normalizer for relative paleointensity estimations and may result in a significant coherence between the NRM/ARM and ARM [Yamazaki, 2008]. However, magnetostatic interaction is not likely to produce important effects in the CADO sediments, which are mostly characterized by PSD ferromagnetic grains. In any case, we conclude that the magnetic susceptibility κ is the best choice for RPI normalization of the sampled sequence, although we recognize that a climatic overprint at eccentricity frequency may affect the reconstructed RPI curve.

A significant coherence appears between ChRM inclination variations and paleointensity (NRM_{20mT}/κ), though no such coherency was observed between ChRM inclination and ARM_{0mT}/κ confirming that shallow inclinations are not influenced by magnetic grain size (Fig.

9B). As expected, there is some coherency and an in-phase relationship between NRM_{20mT}/κ and ARM_{0mT}/κ records in specific intervals of the time series, indicating a magnetic grain size dependency of the RPI record. However, even if the efficiency of the remanence acquisition seems to be influenced by magnetic grain size, the coherency of the computed NRM_{20mT}/κ with the SINT-800 reference curve of Guyodo and Valet [1999] (Fig. 9B) and with the PISO-1500 stack of Channell et al. [2009] (Fig. 9C), over most of the frequency spectrum indicates that the reconstructed geomagnetic RPI variations are significant and can be globally correlated. With the aim to detect the presence of possible periodicities in the time series, standard Fourier spectra were calculated for normalization parameters (ARM_{20mT} and κ), the normalized RPI records (NRM_{20mT}/κ and NRM_{20mT}/ARM_{20mT}) and for ChRM inclination and ARM_{0mT}/κ ratio (Fig. 10). Spectral analysis did not point out any periodicity corresponding to the Milankovitch orbital precession (19-23 ka), obliquity (41 ka) or eccentricity (100 ka) cycles for the normalized RPI curves (NRM_{20mT}/κ and NRM_{20mT}/ARM_{20mT}), but reveals a significant 100 ka periodicity for both the normalizing parameters κ and ARM_{20mT}, with a minor influence of the 41 ka periodicity for the magnetic susceptibility κ. Orbital eccentricity and obliquity periodicities also appear in the ChRM inclination and ARM_{0mT}/κ parameters.

4.4 ChRM inclination, VGP directions and the M-B polarity reversal

Above the reverse to normal polarity transition, the ChRM inclination values fluctuate around a mean value of ca -68°, which is ca 8° shallower than the geomagnetic inclination value of -76.8° expected at the high latitude of the coring site (Fig. 11). Paleomagnetic inclination shallowing is a well known process linked to deposition of magnetic particles and subsequent sediment compaction [Deamer and Kodama 1990; Arason and Levi, 1990]. Shallow bias, or inclination error, has been found in laboratory re-deposition experiments and in some modern natural sediments [see Tauxe and Kent, 1984; 2004; Tan et al., 2003]. The inclination shallowing observed in sediments deposited in saline waters could also be a function of the process of flocculation, which in turn relates to clay content [van Vreumingen, 1993a;b]. A recent numerical modelling of the relationship between inclination shallowing and relative paleointensity in sediments indicates that in absence of inclination shallowing the relative paleointensity recording mechanism may be non-linear [Mitra and Tauxe, 2009]. The occurrence of inclination shallowing appears therefore as a prerequisite for reliable relative paleointensity studies. However, the CADO ChRM inclination record in the interval of constant normal polarity shows some short-lived swings to anomalously low values (i.e. <45° see Fig. 3), that cannot be justified by a sedimentary inclination shallowing only. The frequency of anomalously shallow ChRM inclination data (see histogram of Fig. 11A) is similar to that found on Antarctic lava flows of the Erebus volcanic province [Lawrence et al, 2009], which supports the geomagnetic origin of these features. In the following, we will try to verify if, according to the RPI age model, such shallow ChRM inclinations in the CADO core may correlate to age of known global geomagnetic excursions of the Brunhes Chron [for comprehensive reviews see Langereis et al., 1997; Lund et al., 1998; Singer et al., 2002; Channell, 2006; Thouveny et al., 2004; 2008; Roberts, 2008].

In Fig. 12 the ChRM inclination and the virtual geomagnetic poles (VGP) latitude of the CADO core are plotted versus age and compared to the CADO RPI and the SINT-800 RPI stack, with vertical grey bars drawn to indicate the main intervals of low RPI in the SINT-800 stack of Guyodo and Valet [1999]. The position of the main established geomagnetic excursions for the Brunhes Chron is indicated by arrows, with their estimated age range mostly derived from the Geomagnetic Instability Time Scale (GITS) of Singer et al. [2002; 2008], and the review of Thouveny et al. [2008]. The validated geomagnetic excursions, *sensu* Roberts [2008], are indicated in bold.

Starting from the younger RPI minimum, we observe that a long interval of shallow inclination (up to ca –30°) occurs around 20-35 ka (MAD<1°). This age range includes the occurrence of the Mono Lake excursion whose age has been established at 32 ka by Singer et al. [2008]. According to our reconstructed age model, a data gap occurs around 41 ka, the age of the Laschamp excursion [Guillou et al. 2004]. Lower in the sequence, a distinct sharp shallow inclination peak (up to –42°), corresponding to a broad RPI minimum, occurs at 108 ka, close the age interval assigned to the Blake excursion (ca 110-120 ka, Tric et al. [1991]; Zhu et al. [1994]). All the mentioned shallow ChRM inclination values correspond to intervals with average ARM/κ and MDF_{NRM} values, and are characterized by well defined ChRM with MAD<2°, therefore they do not seem to represent zones of local unusual magnetic mineralogy. On the contrary, other oscillations to anomalously shallow ChRM values (up to ca –35° MAD<1.5°), observed at ca 62 ka, 279 ka and 404 ka, that do not correlate to any of the established Brunhes geomagnetic excursions, correspond to a bioturbated layer with darker mottles, a silty layer and a layer with sparse pebbles, respectively.

Several smoothing processes affect the ability of a sedimentary sequence to record transient geomagnetic features, including smoothing of the geomagnetic signal due to lock-in processes or magnetic mineral reduction related to diagenesis [i.e., deMenocal et al. 1990; Lund and Keigwin, 1994; Tarduno and Wilkison, 1996; Roberts and Winklhofer, 2004; Sagnotti et al., 2005], or due to the instrumental response function of the pick-up coils in the magnetometer [Oda and Shibuya, 1996; Guyodo et al., 2002]. In the CADO core the absence of clear records of many known geomagnetic excursions may probably results from smoothing associated to the relatively low sedimentation rate (on average ca 4.4 cm/kyr) that could be unsuitable to preserve the details of transient geomagnetic field variations [see Lund and Keigwin, 1994; Kent and Schneider, 1995; Roberts and Winklhofer, 2004; Roberts, 2008]. An alternative explanation is that geomagnetic excursions were not globally manifested and they did not produce large deviations from the average geomagnetic field directions at the location of the CADO core. In fact, there is a counter argument in the literature against the significance of post-depositional sedimentary smoothing [e.g. Tauxe et al., 1996; Tauxe, 2006], which supports the hypothesis that the sediment magnetization is locked within the top few centimeters (see the comprehensive review paper by Tauxe and Yamazaki, 2007].

Fig. 13 shows the ChRM inclination, declination, MAD and VGP computed for the bottom (last 100 ka) of the core. The polarity reversal recorded at ca 780 ka can be correlated to the Matuyama-Brunhes (M-B) transition (whose mid-point was dated at ca 789 ka by Quidelleur et al. [2003], at ca 774 ka by Channell et al. [2004], at ca 776 ka by Coe et al. [2004] and Singer et al. [2008]). The M-B transition feature is defined by a reverse- to normal polarity change, taking place within a 27 cm interval, which occurs in a single u-channel and correlates to a RPI minimum [see Kent and Schneider, 1995; Channell et al., 2004]. Taking into account the average sedimentation rate of 4.4 cm/ka calculated by the RPI correlation for this interval, the time it takes for the full directional change corresponds to 6.8 ka, which is comparable to the duration for the M-B reversal proposed in the literature [Tauxe et al., 1996; Coe et al., 2004; Clement 2004; Hyodo et al., 2006].

Below the transition, at ca 790 ka, an abrupt inclination swing, reaching values of the full normal polarity mean (-74°), could be correlated to a globally recognized precursor of the M-B reversal which has been previously reported in deep-sea cores from different oceans and dated from 10 to 17 ka prior to the M-B reversal, with a duration estimated from 2 to 5 ka [Kent and Schneider, 1995; Hartl and Tauxe, 1996; Yamazaki and Oda, 2001, Dinarès-Turell et al., 2002]. The precursor was also radiometrically dated in various volcanic sites with an age range spanning from ca 791-793 to 798 ka [Singer et al., 2002; Coe et al., 2004; Brown et al., 2004]. Considering again a mean sedimentation rate of 4.4 cm/ka for this part of the MD03-2595 CADO core, the duration of the precursor (spanning ca 12 cm of stratigraphic interval) should be ca 2.7 ka, with a time interval between the mid-point of the reversal and the precursor of ca 10 ka. Both are estimates in good agreement with the values reported in the literature [see Channell et al., 2004; Hyodo et al., 2006].

In principle, a delayed lock-in of the remanent natural magnetization in the stratigraphic intervals slightly older than a geomagnetic reversal may cause a record of apparent multiple polarity changes of the ChRM component in a sedimentary sequence [see Spassov et al., 2003]. This process is caused by variable relative contributions of quite different remanence carriers and components during the reversal, and could gives rise to an irregular polarity lock-in at different stratigraphic depths. In the CADO core, however, the homogeneity of the lithology and of all the rock magnetic parameters through the whole core, indicates that a geomagnetic origin of the ChRM oscillation recorded before the M-B transition is by far most likely and we conclude that the CADO core preserves a detailed record of the geomagnetic M-B precursor.

5. Discussion and conclusion

The collection of well defined paleomagnetic data at high-resolution throughout the study sequence, and the consequent compilation of detailed ChRM directions and RPI record, brought important contributions to the reconstruction of the geomagnetic field variability from high latitudes of the southern hemisphere, and therefore to the understanding of the key general features of the Earth's magnetic field within the polar regions.

The CADO RPI curve shows that paleointensity oscillations with periods longer than a few ka can be matched to the global RPI stacks and that a few sharp oscillations to anomalously low ChRM values, occurring during intervals of RPI lows, may represent the smoothed record of geomagnetic excursions or, alternatively, document the occurrence of only limited deviations from average paleomagnetic direction at the site location during the whole Brunhes Chron. In any case, on the whole the paleomagnetic record of the Brunhes Chron does not indicate a substantially larger variability of the geomagnetic field with respect to coeval records from intermediate and low latitudes with comparable sedimentation rates. This is in contrast with the larger variability reported for coeval sediment cores from the Arctic region [e.g. Nowaczyk and Antonow, 1997; Nowaczyk and Frederichs, 1999].

Though the relatively low geomagnetic variability and the relatively modest record of known geomagnetic excursions, the paleomagnetic record of the CADO core preserves a relatively detailed registration of the Matuyama-Brunhes reversal and supports the global existence of a precursor preceding by a few ka the full major reversal. As a result, this record represents the southernmost registration of the M-B transition and its precursor and indicates that the timing, rate and dynamics of such reversal and event, at high southern latitudes, are not substantially different from those reconstructed elsewhere.

In addition, orbital periodicities (100 ka and 41 ka) are found for the ChRM paleomagnetic inclination record, which are similar to those reported for other sedimentary cores at low-latitudes [Yamazaki and Oda 2002; 2004]. These data support the model of Yamazaki and Oda [2002], which suggests a connection between the geodynamo and the orbital eccentricity, indicating that long-term geomagnetic secular variation in inclination are controlled by changes in the relative strength of the geocentric axial dipole and persistent non-dipole components. The significant coherence between ChRM inclination variations and paleointensity (NRM_{20mT}/κ) are also similar to those obtained on a sediment core from the western equatorial Pacific by Yamazaki and Oda [2002; 2004] and indicates that shallower (steeper) inclinations may correlate with paleointensity minima (maxima).

Finally, rock magnetic data from the CADO core indicate a substantial uniformity of concentration, composition and grain size of the magnetic minerals contained in the study sequence. On the one hand, this uniformity is consistent with the observed homogeneity of sedimentary facies and indicates that the alternation of paleoclimatic phases that characterized the last ca 800 ka did not produce pronounced oscillations in the environmental magnetic proxies at the core location. This result matches the previous findings of Macrì et al. [2005] for shorter cores from the WLB and indicates a substantial stability of the East Antarctic Ice Sheet during the middle and late Pleistocene. On the other hand, a climatic periodicity of 100 ka is detectable in the κ and ARM_{20mT} parameters, together with a minor contribution of the 41 ka obliquity periodicity for the κ and κARM_{0mT} /κ parameters**,** indicating that subtle variations linked to orbital cycle affect the concentration and grain-size of the magnetic particles in the study sequence.

Acknowledgments

The MD03-2595 CADO core was studied as part of the QUASAR (QUAternary Sedimentary processes on the east Antarctic continental Rise) project that was funded by the PNRA (*Programma Nazionale di Ricerche in Antartide*). Members of the QUASAR working group are acknowledge for help with continued discussion on core stratigraphy and sedimentology. We thank two anonymous reviewers for their comments and suggestions, which allowed to improve the manuscript.

References

Arason, P., and Levi, S., 1990. Compaction and inclination shallowing in deep-sea sediments from the Pacific Ocean. J. Geophys. Res., 95: 4501–4510.

Aurnou, J.M., Andreadis, S., Zhu, L., and Olson, P.L., 2003. Experiments on convection in Earth's core tangent cylinder. Earth Planet. Sci. Lett., 212: 119-134.

Biggin, A.J., Strik, G.H.M.A., and Langereis C.G., 2009. The intensity of the geomagnetic field in the late-Archaean: new measurements and an analysis of the updated IAGA palaeointensity database. Earth Planets Space, 61: 9–22.

Brachfeld, S.A., Acton, G.D., Guyodo, Y., and Banerjee, S.K., 2000. High-resolution paleomagnetic records from Holocene sediments from the Palmer Deep, western Antarctic Peninsula. Earth Planet. Sci. Lett., 181: 421-441.

Brachfeld, S.A., Domack, E.W., Kissel, C., Laj, C. Leventer, A., Ishman, S.E., Gilbert, R., Camerlenghi, A., and Eglinton, L.B., 2003. Holocene History of the Larsen Ice Shelf Constrained by Geomagnetic Paleointensity Dating, Geology, 31: 749-752.

Brancolini, G., and Harris, P.T., 2000. Post Cruise Report AGSO Survey 217: Joint Italian/Australian Marine Geoscienze Expedition Aboard the R.V. Tangaroa to the Geotge Vth Land Region of East Antartica during February-March, 2000. Australian National Antarctic Research Expeditions Project No. 1044, Wilkes Land Glacial History (WEGA), AGSO Record.

Brown, L.L., Singer, B.S., Pickens, J.C., and Jicha, B.R. 2004. Paleomagnetic directions and 40Ar//39Ar ages from the Tatara-San Pedro volcanic complex, Chilean Andes: Lava record of a Matuyama-Brunhes precursor? Journal of Geophys. Res., Vol. 109, B12101, doi:10.1029/2004JB003007.

Busetti, M., Caburlotto, A., Armand, L., Damiani, D., Giorgetti, G., Lucchi, R.G., Quilty, P.G., and Villa, G., 2003. Plio-Quaternary sedimentation on the Wilkes land continental rise: preliminary results. Deep-Sea Research II, 50: 1529–1562.

Caburlotto, A., Macrì, P., Damiani, D., Giorgetti, G., Busetti, M., Villa, G., and Lucchi, R.G., 2003. Piston cores from the Wilkes Land Rise: Data and Considerations. Terra Antartica Reports, 9: 63-68.

Channell, J.E.T., Curtis, J.H., and Flower, B.P., 2004. The Matuyama-Brunhes boundary interval (500-900 ka) in North Atlantic drift sediments. Geophys. J. Int., 158: 489-505.

Channell, J.E.T., 2006. Late Brunhes polarity excursions (Mono Lake, Iceland Basin and Pringle Falls) recorded at ODP Site 919 (Irminger Basin). Earth Planet. Sci. Lett., 244: 378-393.

Channell, J.E.T., Xuan C., and Hodell, D.A., 2009. Stacking paleointensity and oxygen isotope data for the last 1.5 Myr (PISO-1500). Earth Planet. Sci. Lett., 283: 14-23.

Clement, B.M., 2004. Dependence of the duration of geomagnetic polarity reversals on site latitude. Nature, 428: 637-640.

Coe, R.S., Singer, B.S., Pringle, M.S., and Zhao X., 2004. Matuyama–Brunhes reversal and Kamikatsura event on Maui: paleomagnetic directions, 40Ar/39Ar ages and implications. Earth Plan. Sci. Lett., 222: 667-684.

Day, R., Fuller, M., and Schmidt, V.A., 1977. Hysteresis properties of titanomagnetites. Grain-size and compositional dependence. Phys. Earth Planet. Int., 13: 260–267.

Deamer, G.A., and Kodama, K.P., 1990. Compaction-induced inclination shallowing in synthetic and natural clay-rich sediments. J. Geophys. Res., 95(B4): 4511-4529.

deMenocal, P.B., Ruddiman W.F., and Kent D.V., 1990. Depth of post-depositional remanence acquisition in deep-sea sediments: a case study of the Brunhes-Matuyama reversal and oxygen isotopic Stage 19.1. Earth and Planet. Sci. Lett., 99: 1-13.

Dinarès-Turell, J., Sagnotti, L., and Roberts, A.P., 2002. Relative geomagnetic paleointensity from the Jaramillo Subchron to the Matuyama/Brunhes boundary as recorded in a Mediterranean piston core. Earth Planet. Sci. Lett., 194: 327-341.

Escutia, C., Eittreim, S.L., and Cooper, A.K., 1997. Cenozoic Sedimentation on the Wilkes Land Continental Rise, Antarctica. In C.A., Ricci (Ed.) Proceedings of the VII International Symposium on Antarctic Earth Sciences. Terra Antarctica Publication, Siena: 791-795.

Fisher, R.A., 1953. Dispersion on a sphere. Proc. R. Soc. London, 217: 295-305.

Glatzmaier, G.A., and Roberts, P.H,. 1995a. A three-dimensional convective dynamo solution with rotating and finitely conducting inner core and mantle. Phys. Earth Planet. Int., 91: 63-75.

Glatzmaier, G.A., and Roberts, P.H., 1995b. A Three-Dimensional Self-Consistent Computer Simulation of a Geomagnetic Field Reversal. Nature, 377: 203-209.

Guillou, H., Singer, B., Laj, C., Kissel, C., Scaillet, S., and Jicha, B.R., 2004. On the age of the Laschamp geomagnetic excursion. Earth Planet. Sci. Lett., 227: 331–343.

Guyodo, Y., and Valet, J.-P., 1999. Global changes in geomagnetic intensity during the past 800 thousand years. Nature, 399: 249-252.

Guyodo, Y., Acton, G.D., Brachfeld, S., and Channell, J.E.T., 2001. A sedimentary paleomagnetic record of the Matuyama chron from the Western Antarctic Margin (ODP Site 1101). Earth Planet. Sci. Lett. 191:61–74.

Guyodo, Y., Channell, J.E.T. and Thomas Ray, G., 2002. Deconvolution of u-channel paleomagnetic data near geomagnetic reversals and short events. Geoph. Res. Lett., 29, 1845, doi: 10.1029/2002GL014927.

Hartl, P., and Tauxe, L., 1996. A precursor to the Matuyama/Brunhes transition-field instability as recorded in pelagic sediments. Earth Plan. Sci. Lett., 138: 121-135.

Hyodo, M., Biswas, D.K., Noda, T., Tomioka, N., Mishima, T., Itota, C., and Sato, H., 2006. Millennial- to submillennial-scale features of the Matuyama-Brunhes geomagnetic polarity transition from Osaka Bay, southwestern Japan. J. Geoph. Res., 111, B02103, doi:10.1029/2004JB003584.

Kent, D.V., and Schneider, D.A., 1995. Correlation of paleointensity variation records in the Brunhes/Matuyama polarity transition interval. Earth Planet. Sci. Lett., 129: 135-144.

King, J.W., Banerjee, S.K., and Marvin, J., 1983. A new rock-magnetic approach to selecting sediments for geomagnetic paleointensity for the last 4000 years. J. Geophys. Res., 88(B7): 5911-5921.

Kirschvink, J.L., 1980. The least-squares line and plane and the analysis of paleomagnetic data. Geophys. J. Roy. Astron. Soc., 62: 699-718.

Kuang, W., and Bloxham, J., 1997. An Earth-like numerical dynamo model. Nature, 389: 371-374.

Langereis, C.G., Dekkers, M.J., de Lange, G.J., Paterne, M.E., and van Santvoort, P.J.M., 1997. Magnetostratigraphy and astronomical calibration of the last 1.1 Myr from an eastern Mediterranean piston core and dating of short events in the Brunhes. Geophys. J. Int., 129: 75-94.

Lawrence, K. P., Tauxe, L., Staudigel, H., Constable, C.G., Koppers, A., McIntosh, W., and Johnson C.L., 2009. Paleomagnetic field properties at high southern latitude, Geochem. Geophys. Geosyst., 10, Q01005, doi:10.1029/2008GC002072.

Lund, S.P., and Keigwin, L., 1994. Measurement of the degree of smoothing in sediment paleomagnetic secular variation records: an example from Late Quaternary deep-sea sediments of the Bermuda Rise, western North Atlantic Ocean. Earth Planet. Sci. Lett., 122: 317–330.

Lund, S.P., Acton, G., Clement, B., Hastedt, M., Okada, M., and Williams, R., 1998. Geomagnetic field excursions occurred often during the last million years. EOS, Trans. Am. Geophys. Un., 79: 178-179.

Macrì, P., Sagnotti, L., Dinares-Turell, J., and Caburlotto, A., 2005. A composite record of Late Pleistocene relative geomagnetic paleointensity from the Wilkes Land Basin (Antarctica). Phys. Earth Planet. Int., 151: 223–242.

Macrì, P., Sagnotti, L., and Lucchi, R.G., 2006. A stacked record of relative geomagnetic paleointensity for the past 270 kyr from the western continental rise of the Antarctic Peninsula. Earth Planet. Sci. Lett., 252: 162-179.

Meynadier, L., Valet, J.-P., Weeks, R., Shackleton, N.J., and Hagee, V.L., 1992. Relative geomagnetic intensity of the field during the last 140 ka. Earth Planet. Sci. Lett., 114: 39-57.

Mitra, R. and Tauxe, L., 2009. Full vector model for magnetization in sediments. Earth Planet. Sci. Lett., 286: 535-545.

Nowaczyk, N.R., and Antonow, M., 1997. High resolution magnetostratigraphy of four sediment cores from the Greenland Sea - I. Identification of the Mono Lake excursion, Laschamp and Biwa I/Jamaica geomagnetic polarity events. Geophys. J. Int., 131: 310–324.

Nowaczyk, N., and Frederichs, T., 1999. Geomagnetic events and relative paleointensity variations during the last 300 ka as recorded in Kolbeinsey Ridge sediments, Iceland Sea, indication for a strongly variable geomagnetic field. Int. J. Earth Sci., 88: 116–131.

Oda, H., and Shibuya, H., 1996. Deconvolution of long-core paleomagnetic data of Ocean Drilling Program by Akaike's Bayesian Information Criterion minimization. J. Geophys. Res., 101: 2815-2834.

Paillard, D., Labeyrie, L., and Yiou, P., 1996. Macintosh program performs time-series analysis. Eos, Trans. Am. Geophys. Un., 77: 397.

Perrin, M., and Schnepp, E., 2004. IAGA paleointensity database: Distribution and quality of the data set. Phys. Earth Planet. Int., 147(2-3): 255-267.

Quidelleur, X., Carlut, J., Soler, V., Valet, J.-P., and Gillot, P.-Y., 2003. The age and duration of the Matuyama-Brunhes transition from new K-Ar data from La Palma (Canary Islands) and revisited 40Ar/39Ar ages. Earth Planet. Sci. Lett., 208: 149-163.

Rebesco, M., Larter, R.D., Barker, P.F., Camerlenghi, A., and Vanneste, L.E., 1997. The history of sedimentation on the continental rise west of the Antarctic Peninsula. In Cooper A.K. and P.F. Barker (Eds), Geology and seismic stratigraphy of the Antarctic margin, Part 2. Antarctic Research Series 71, American Geophysical Union, Washington DC: 29-49.

Roberts, A.P., and Winklhofer, M., 2004. Why are geomagnetic excursions not always recorded in sediments? Constraints from post-depositional remanent magnetization lock-in modelling. Earth Planet. Sci. Lett., 227: 345-359.

Roberts, A.P., 2006. High-resolution magnetic analysis of sediment cores: Strengths, limitations and strategies for maximizing the value of long-core magnetic data, Phys. Earth Planet. Int., 156: 162–178.

Roberts, A.P., 2008. Geomagnetic excursions: knowns and unknowns. Geophys. Res. Lett., 35, L17307, doi:10.1029/2008GL034719.

Sagnotti, L., Macrì, P., Camerlenghi, A., and Rebesco M., 2001. Environmental magnetism of late Pleistocene sediments from the pacific margin of the Antarctic Peninsula and interhemispheric correlation of climatic events. Earth Planet. Sci. Lett., 192: 65-80.

Sagnotti, L., Rochette, P., Jackson, M., Vadeboin, F., Dinarès-Turell, J., Winkler, A., and "Mag-Net" Science Team, 2003. Inter-laboratory calibration of low field magnetic and anhysteretic susceptibility measurements. Phys. Earth Planet. Int., 138: 25–38.

Sagnotti, L., Budillon, F., Dinarès-Turell, J., Iorio, M., and Macrì, P., 2005. Evidence for a variable paleomagnetic lock-in depth in the Holocene sequence from the Salerno Gulf (Italy): implications for "high-resolution" paleomagnetic dating, Geochem. Geophys. Geosyst., 6, doi:10.1029/2005GC001043.

Singer, B.S., Relle, M.K., Hoffman, K.A., Battle, A., Laj, C., Guillou, H., and Carracedo J.C., 2002. Ar/Ar ages from transitionally magnetized lavas on La Palma, Canary Islands, and the geomagnetic instability timescale. J. Geophys. Res., 107: 2307, doi: 10.1029/2001JB001613.

Singer, B.S., Jicha, B.R., Kirby, B.T., Geissman, J.W., and Herrero-Bervera, E., 2008. 40Ar/39Ar dating links Albuquerque Volcanoes to the Pringle Falls excursion and the Geomagnetic Instability Time Scale. Earth Planet. Sci. Lett., 267: 584–595.

Spassov, S., Heller, F., Evans, M.E., Yue, L.P., von Dobeneck, T., 2003. A lock-in model for the complex Matuyama-Brunhes boundary record of the loess/palaeosol sequence at Lingtai (Central Chinese Loess Plateau). Geophys. J. Int., 155, (2): 350-366.

Stacey, F.D., and Banerjee, S.K., 1974. The physical principles of rock magnetism. Elsevier, Amsterdam,195 p.

Stoner, J.S., Laj, C., Channell, J.E.T., and Kissel, C., 2002. South Atlantic and North Atlantic geomagnetic paleointensity stacks (0-80 ka): implications for inter-hemispheric correlation. Quat. Sci. Rev., 21:1141-1151.

Stoner, J.S., Channell, J.E.T., Hodell, D.A., and Charles, C.D., 2003. A ~570-kyr geomagnetic paleosecular variation record from the sub-Antarctic South Atlantic (ODP Site 1089). J. Geophys. Res., 108 (B5):2242, doi:10.1029/2001JB001390

Sugiura, N., 1979. ARM, TRM and magnetic interactions: concentration dependence, Earth Planet. Sci. Lett., 42: 451-455.

Tan, X.D., Kodama, K.P., Chen, H.L., Fang, D.J., Sun, D.J., and Li, Y.A., 2003. Paleomagnetism and magnetic anisotropy of Cretaceous red beds from the Tarim basin, northwest China: Evidence for a rock magnetic cause of anomalously shallow paleomagnetic inclinations from central Asia. J. Geophys. Res.,108, 2107, doi:10.1029/2001JB001608.

Tarduno, J.A., and Wilkison, S.L., 1996. Non-steady state magnetic mineral reduction, chemical lock-in, and delayed remanence acquisition in pelagic sediments. Earth Planet. Sci. Lett., 144: 315-326.

Tauxe, L., and Kent, D.V., 1984. Properties of a detrital remanence carried by haematite from study of modern river deposits and laboratory redeposition experiments. Geophys. J. R. Astr. Soc., 77: 543–561.

Tauxe, L., 1993. Sedimentary records of relative paleointensity of the geomagnetic field: theory and practice. Rev. Geophys., 31: 319-354.

Tauxe, L., Herbert, T., Shackleton, N.J., and Kok, Y.S., 1996. Astronomical calibration of the Matuyama-Brunhes boundary: Consequences for magnetic remanence acquisition in marine carbonates and the Asian loess sequences. Earth Planet. Sci. Lett., 140: 133–146.

Tauxe, L., and Kent, D.V., 2004. A simplified statistical model for the geomagnetic field and the detection of shallow bias in paleomagnetic inclinations: Was the ancient magnetic field dipolar? In Timescales of the Paleomagnetic field, Channell, J.E.T. et al., eds., Geophysical Monograph, 145: 101-116.

Thouveny, N., Carcaillet, J., Moreno, E., Leduc, G., and Nérini, D., 2004. Geomagnetic moment variation and paleomagnetic excursions since 400 ka BP: a stacked record of sedimentary sequences of the Portuguese margin. Earth Planet.Sci.Lett., 219: 377-396.

Tauxe L (2006) Long term trends in paleointensity: The contribution of DSDP/ODP submarine basaltic glass collections. Physics of the Earth and Planetary Interiors, 156: 223–241.

Tauxe, L., and Yamazaki, T., 2007. Paleointensities. In Schubert, G., (Ed.), Treatise on Geophysics, vol.5, Geomagnetism. Elsevier Ltd, Oxford: 509–564.

Thouveny, N., Bourlès, D.L., Saracco, G., Carcaillet, J.T., and Bassinot, F., 2008. Paleoclimatic context of geomagnetic dipole lows and excursions in the Brunhes, clue for an orbital influence on the geodynamo? Earth Planet. Sci. Lett., 275: 269-284.

Tric, E., Laj, C., Valet, J.-P., Tucholka, P., Paterne, M., and Gichard, F., 1991. The Blake geomagnetic event: transition geometry, dynamical characteristics and geomagnetic significance. Earth Planet. Sci. Lett., 102: 1-13.

Valet, J.P., Meynadier, L., Bassinot, F.C., and Garnier, F., 1994. Relative paleointensity across the last geomagnetic reversal from sediments of the Atlantic, Indian and Pacific Oceans. Geoph. Res. Lett., 21(6): 485-488.

Valet, J.-P., and Meynadier, L., 1998. A comparison of different techniques for relative paleointensity. Geophys. Res. Lett., 25: 89-92.

van Vreumingen, M.J., 1993a. The Influence of Salinity and Flocculation Upon the Acquisition of Remanent Magnetization in Some Artificial Sediments. Geophys. J. Int. 114 (3), 607–614.

van Vreumingen, M.J., 1993b. The Magnetization Intensity of Some Artificial Suspensions While Flocculating in a Magnetic-Field. Geophys. J. Int. 114 (3), 601–606.

Zhu, R.X., Zhou, L.P., Laj, C., Mazaud, A., and Ding, Z.L., 1994. The Blake geomagnetic episode recorded in Chinese loess. Geophys. Res. Lett., 21: 697-700.

Yamazaki, T., and Ioka, N., 1997. Cautionary note on magnetic grain-size estimation using the ratio of ARM to magnetic susceptibility. Geophys. Res. Lett., 24: 751-754.

Yamazaki, T., and Oda, H., 2001. A Brunhes-Matuyama polarity transition record from anoxic sediments in the South Atlantic (Ocean Drilling Program Hole 1082C). Earth Planets Space, 53: 817-827.

Yamazaki, T., and Oda, H., 2002. Orbital influence on Earth's magnetic field: 100,000-year periodicity in inclination. Science, 295: 2435-2438.

Yamazaki, T., and Oda H., 2004. Intensity-Inclination Correlation on Long-Term Secular Variation of the Geomagnetic Field and its Relevance to Persistent Non-Dipole Component. AGU Monograph 145 "Timescales of the Internal Geomagnetic Field": 287-298.

Yamazaki, T., 2008. Magnetostatic interactions in deep-sea sediments inferred from first-order reversal curve diagrams: Implications for relative paleointensity normalization. Geochem. Geophys. Geosyst., 9, doi: Q02005, doi:10.1029/2007GC001797.

Figure captions

Fig. 1 – A) Bathymetric map of the continental rise of the Wilkes Land Basin: the morphology of the rise is characterized by a channel-ridge system elongated perpendicular to the margin. Points aligned on acoustic Line 26 shows the location of the previously studied WEGA cores (see text). B) 3.5 kHz acoustic profile crossing the Buffon Canyon (Line W39) with location of the MD03- 2595 core. Redrawn from Busetti et al. (2003).

Fig. 2 – Typical alternating field (AF) demagnetization behavior at selected depths of the MD03- 2593 core. Paleomagnetic data indicate that, after removal of a viscous component at AF < 10-20 mT, a characteristic remanent magnetization (ChRM) can be easily identified. Orthogonal vector diagrams: open and closed symbols represent projections onto vertical and horizontal planes, respectively. Equal area projections: open (close) symbols represent projection onto the upper (lower) hemisphere.

Fig. 3 – Paleomagnetic directions, maximum angular deviation (MAD) [Kirschvink, 1980] and the normalized relative paleointensity curves NRM_{20mT}/κ and NRM_{20mT}/ARM_{20mT} for the CADO core. The u-channel sections (1 to 24) are indicated to the right of the lithostratigraphic column. The dashed lines on the ChRM declination and inclination plots indicate the expected value of the declination (360°) and inclination (-76.8°) at the core location.

Fig. 4 – Downcore variation of the main rock magnetic parameters measured for the CADO core. The little squares on the right of the lithostratigraphic column indicate the position of the 8

sub-samples selected for rock magnetic analysis. Horizontal gray bars in the plots indicate the position of silty clays and laminated muds.

Fig. 5 –Thermomagnetic curves of the samples selected for rock magnetic analyses, showing the variation in the magnetic susceptibility (κ) with temperature in heating-cooling cycles from room temperature to 700°C. The sharp drop at ca 580°C in all the heating curves indicates the presence of magnetite, whereas the thermal instability between 250 and 350°C suggests the presence of maghemite which is converted to hematite during the thermal treatment. The cooling path is always well above of the heating path and indicates that new magnetite is produced by thermal alteration during heating.

Fig. 6 - A) and B) Representative hysteresis loops and C) B_{cr}/B_c vs M_r/M_s plot [Day et al. 1977] for the selected specimens of the CADO core. B_{cr}: remanent coercive force, B_c: coercive force, M_r: saturation remanent magnetization, M_s: saturation magnetization. Hysteresis parameters were computed after correction for the high-field paramagnetic slope. SD= single domain, PSD= pseudo single domain, and MD= multidomain grains.. D) The ARM/κ ratio, indicates a substantial uniformity in magnetic mineral grain size, apart from a few data from distinct intervals, which were disregarded for RPI analyses

Fig. 7 – SINT-800 reference curve of Guyodo and Valet [1999] and the CADO RPI record (NRM_{20mT}/k). Vertical lines indicate tie points used for correlation. B) After correlation the CADO RPI curve was scaled to its maximum value and plotted together with the SINT-800. The correlation indicates that the CADO core reaches back to ca 800 ka. C) Downcore variation of the sedimentation rates obtained with the RPI-based age model for the CADO core. Unbroken line is age versus depth, broken line is depth versus sedimentation rate calculated between the RPI tie points.

Fig. 8 – Comparison of the CADO RPI curve with the SINT-800 and the PISO-1500 global RPI stacks and with other southern high-latitude RPI records extracted from the MagIC database, in the interval 0-800 ka. Sint-800 from Guyodo and Valet, [1999], PISO-1500 from Channell et al., [2009], Core 1089 from Stoner et al. [2003], Ks87-752 from Valet et al. [1994], 5-pc01 from Stoner et al. [2002], Core 1101 from Guyodo et al. [2001], Core PC20 from Macrì et al. [2005].

Fig. 9 – Spectral analysis performed using Blackman-Tukey method with a Bartlett window. A) Square coherence and phase for the RPI curves with respect to each other and with respect to the normalization parameters. B) Square coherence and phase for the ChRM inclination with respect to the NRM_{20mT}/κ RPI record and the ARM_{0mT}/κ ratio, and for the NRM_{20mT}/κ RPI record with respect to the ARM_{0mT}/κ ratio and the reference SINT-800 stack. B) Square coherence and phase between CADO and PISO-1500 RPI records. See text for explanation.

Fig. 10 – Standard spectra of the parameters used for the RPI normalisation (κ and ARM), the normalized relative paleointensity curves (NRM_{20mT}/κ and NRM_{20mT}/ARM_{20mT}), ARM_{0mT}/κ and the ChRM inclination.

Fig. 11 – A) Histograms of ChRM inclinations and declinations. N is the number of data. Expected normal and reverse inclinations at the CADO latitude site are shown as a vertical dashed lines. B) Equal-area projections of paleomagnetic directions. D and I are mean declination and inclination calculated using Fisher's statistics [Fisher 1953] on the not-transitional and not-excursional normal and reverse ChRM directions (i.e. directions providing a VGP latitude greater than ± 45°), with uncertainties estimated by the α_{95} parameter.

Fig. 12 – CADO RPI record and SINT-800 of Guyodo and Valet [1999], compared with ChRM inclination record and VGP latitude of the CADO core. The black arrows indicate geomagnetic excursions recognized in the literature, with the validated excursions, *sensu* Roberts [2008], indicated in bold (see text). The grey vertical areas correspond to the main RPI minima in the SINT-800 record of Guyodo and Valet [1999].

Fig. 13 – ChRM directions, MAD and VGP latitude for the bottom part of the CADO core (interval dated at 750-800 ka). Vertical dashed lines correspond to the u-channel breaks. The gray area shows the interval that was correlated to the uppermost part of the reverse Matuyama Chron preserving a record of the Matuyama-Brunhes transition and of its precursor. See text for discussion.

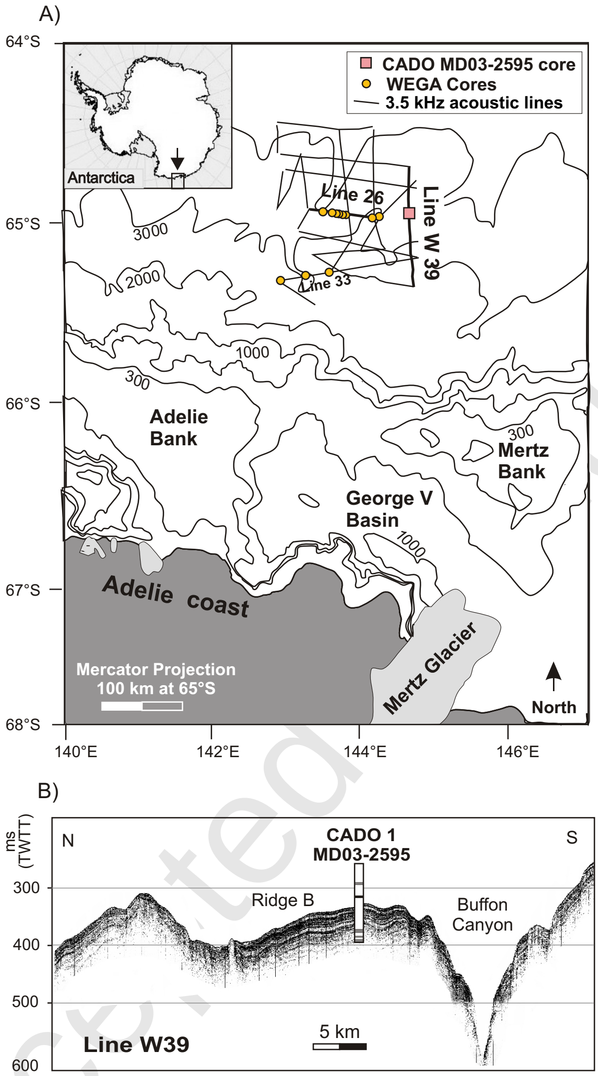
A)
64°S
65°S
66°S
67°S
68°S
140°E
142°E
144°E
146°E
CADO MD03-2595 core
WEGA Cores
3.5 kHz acoustic lines
Antarctica
Line 26
Line W 39
Line 33
3000
2000
1000
300
Adelie Bank
Mertz Bank
George V Basin
Adelie coast
Mertz Glacier
Mercator Projection
100 km at 65°S
North
B)
ms (TWTT)
N
S
CADO 1
MD03-2595
Ridge B
Buffon Canyon
300
400
500
600
Line W39
5 km

Fig. 1

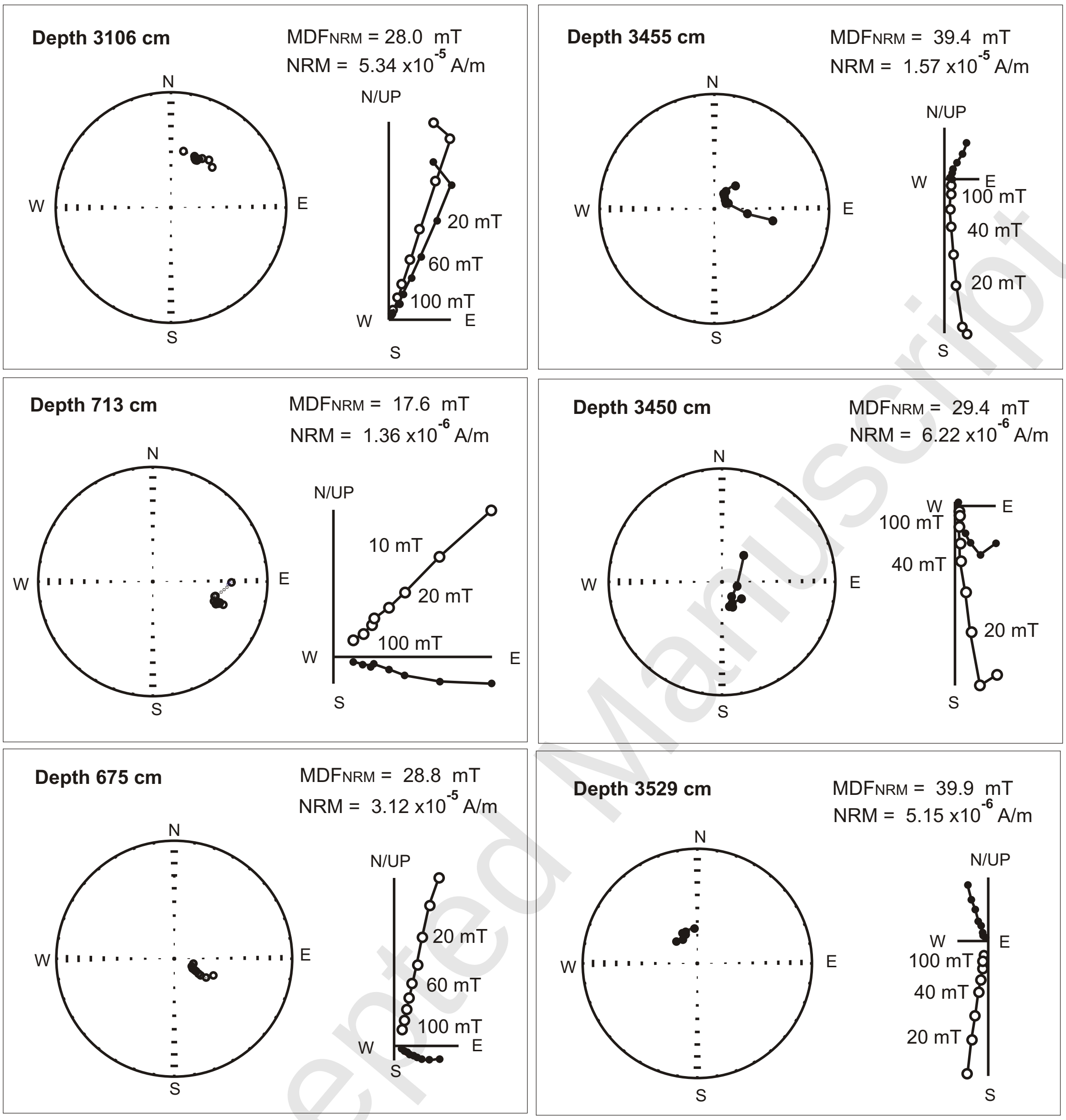

Depth 3106 cm
MDFNRM = 28.0 mT
NRM = 5.34 x10-5 A/m
N
W
E
S
N/UP
20 mT
60 mT
100 mT
W
E
S
Depth 3455 cm
MDFNRM = 39.4 mT
NRM = 1.57 x10-5 A/m
N
W
E
S
N/UP
W
E
100 mT
40 mT
20 mT
S
Depth 713 cm
MDFNRM = 17.6 mT
NRM = 1.36 x10-6 A/m
N
W
E
S
N/UP
10 mT
20 mT
100 mT
W
E
S
Depth 3450 cm
MDFNRM = 29.4 mT
NRM = 6.22 x10-6 A/m
N
W
E
S
W
E
100 mT
40 mT
20 mT
S
Depth 675 cm
MDFNRM = 28.8 mT
NRM = 3.12 x10-5 A/m
N
W
E
S
N/UP
20 mT
60 mT
100 mT
W
E
S
Depth 3529 cm
MDFNRM = 39.9 mT
NRM = 5.15 x10-6 A/m
N
W
E
S
N/UP
W
E
100 mT
40 mT
20 mT
S

Fig. 2

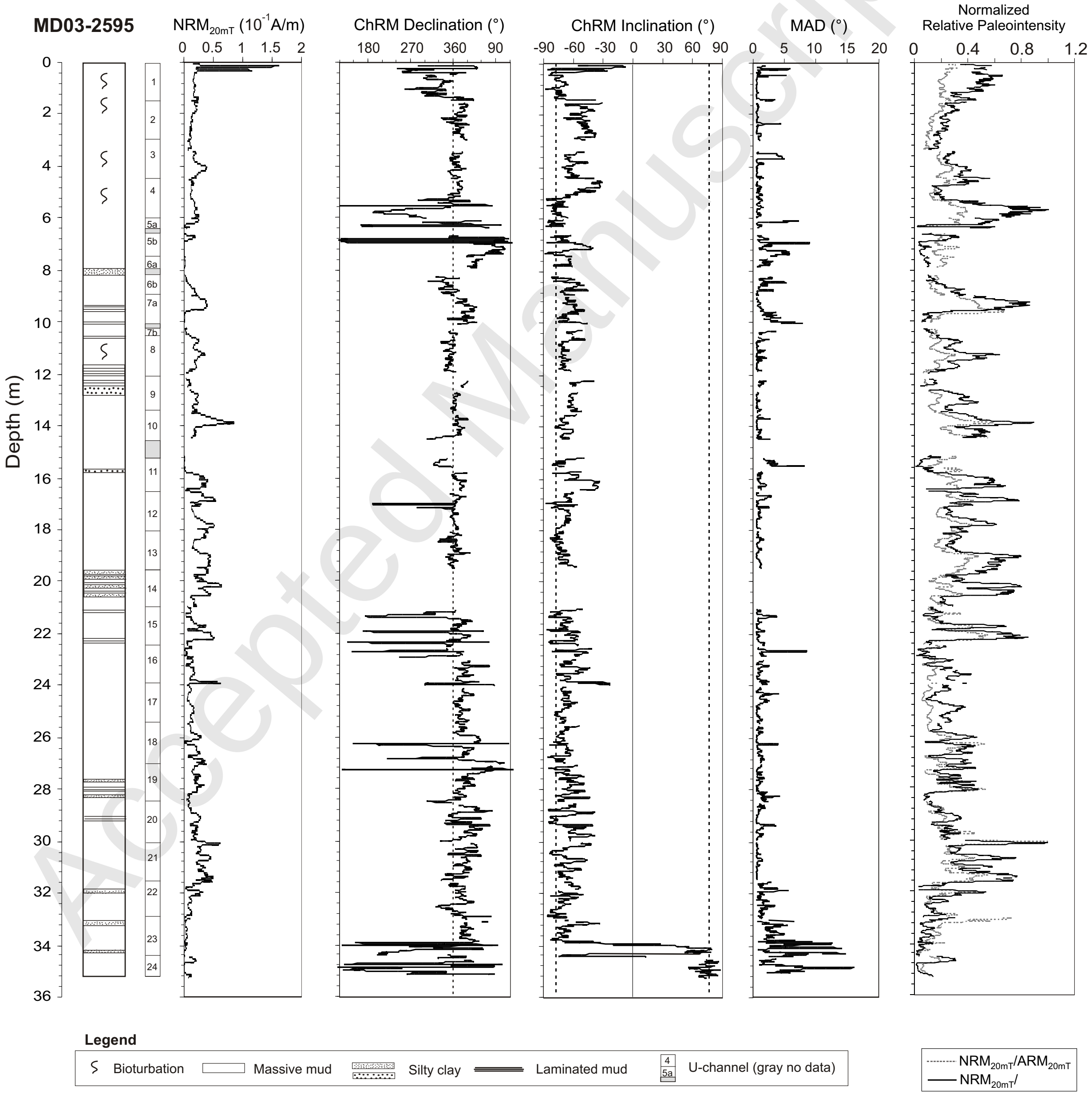

MD03-2595
NRM20mT (10-1A/m)
ChRM Declination (°)
ChRM Inclination (°)
MAD (°)
Normalized Relative Paleointensity
Depth (m)
Legend
Bioturbation
Massive mud
Silty clay
Laminated mud
U-channel (gray no data)
NRM20mT/ARM20mT
NRM20mT/

Fig. 3

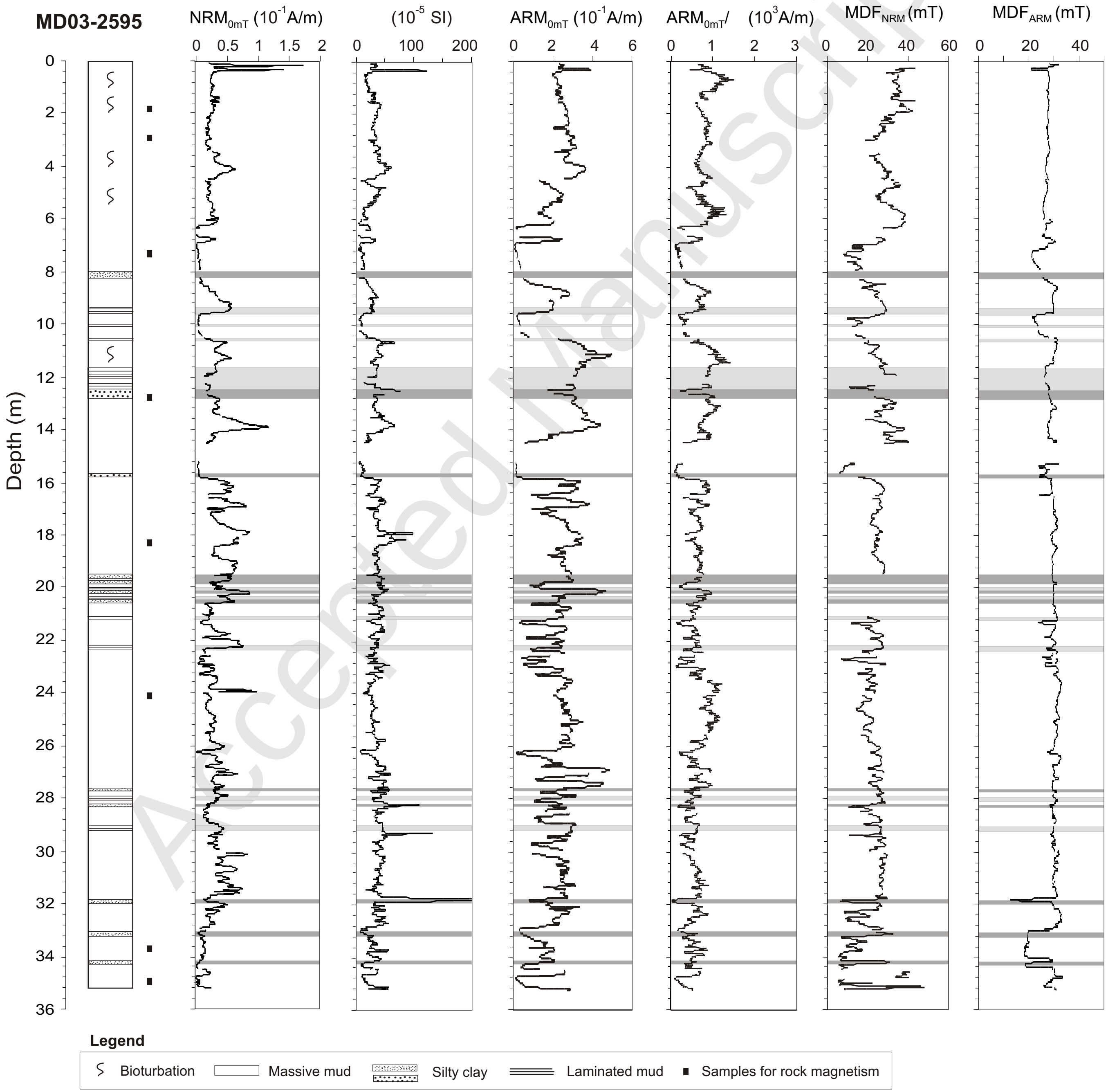

MD03-2595
NRM0mT (10-1A/m)
(10-5 SI)
ARM0mT (10-1A/m)
ARM0mT/ (103A/m)
MDFNRM (mT)
MDFARM (mT)
Depth (m)
Legend
Bioturbation
Massive mud
Silty clay
Laminated mud
Samples for rock magnetism

Fig. 4

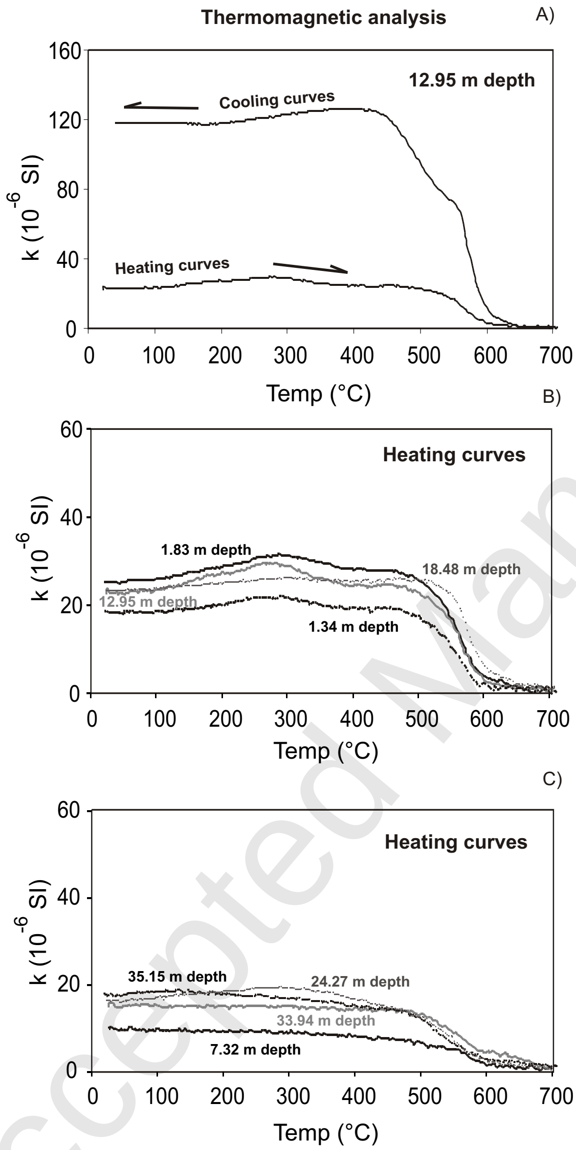

Thermomagnetic analysis
A)
12.95 m depth
Cooling curves
Heating curves
k (10-6 SI)
160
120
80
40
0
0
100
200
300
400
500
600
700
Temp (°C)
B)
Heating curves
1.83 m depth
18.48 m depth
12.95 m depth
1.34 m depth
60
40
20
C)
Heating curves
35.15 m depth
24.27 m depth
33.94 m depth
7.32 m depth

Fig. 5

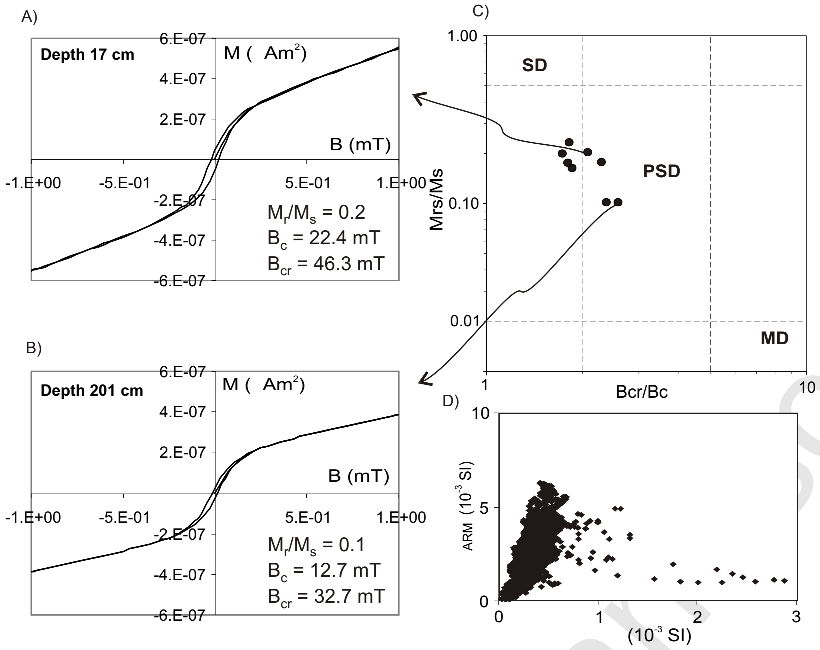

A)
Depth 17 cm
M (Am²)
B (mT)
Mr/Ms = 0.2
Bc = 22.4 mT
Bcr = 46.3 mT
B)
Depth 201 cm
M (Am²)
B (mT)
Mr/Ms = 0.1
Bc = 12.7 mT
Bcr = 32.7 mT
C)
SD
PSD
MD
Mrs/Ms
Bcr/Bc
D)
ARM (10⁻³ SI)
(10⁻³ SI)

Fig. 6

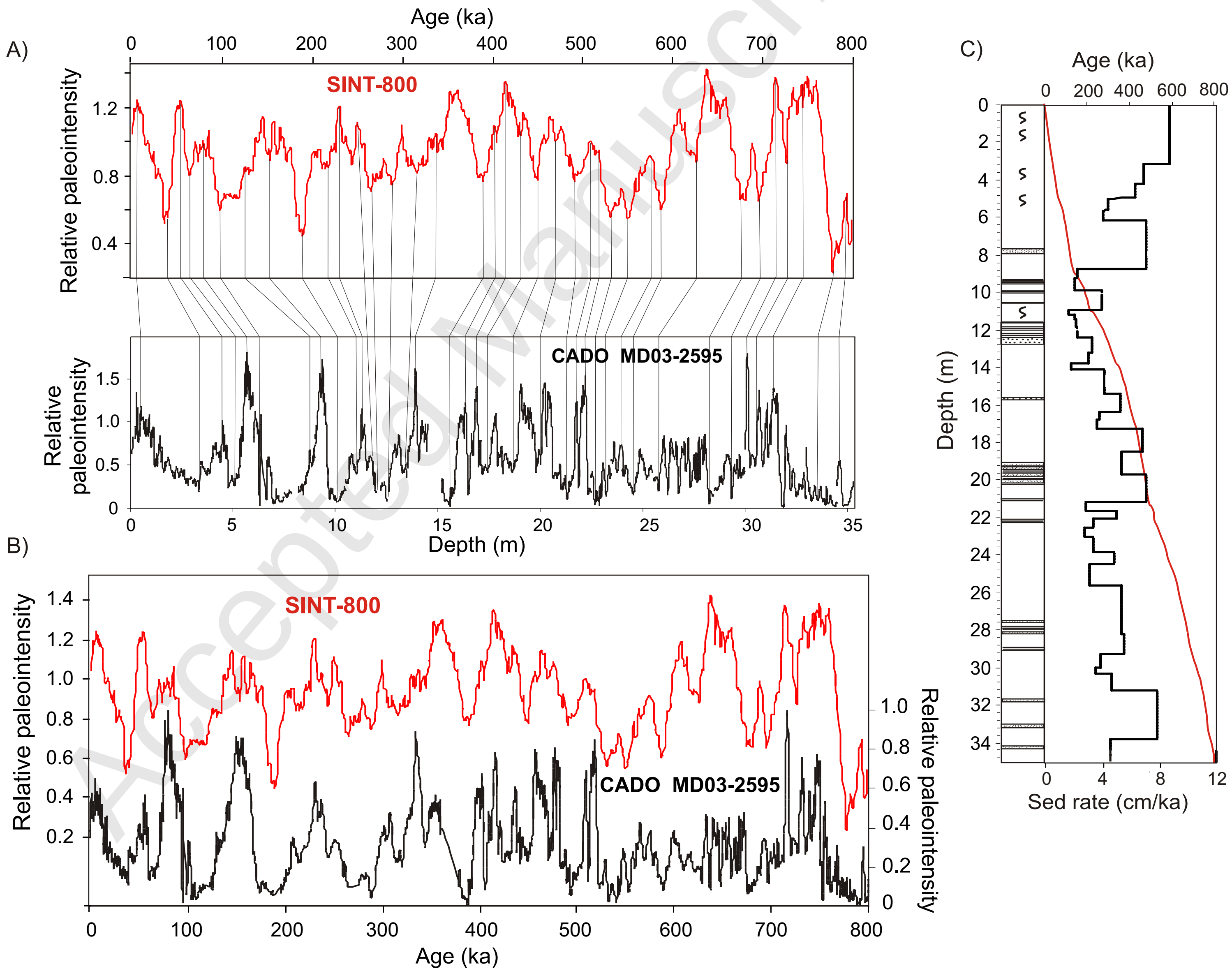
A)
Age (ka)
0
100
200
300
400
500
600
700
800
SINT-800
Relative paleointensity
1.2
0.8
0.4
CADO MD03-2595
Relative paleointensity
1.5
1.0
0.5
0
Depth (m)
5
10
15
20
25
30
35
B)
SINT-800
Relative paleointensity
1.4
1.2
1.0
0.8
0.6
0.4
0.2
CADO MD03-2595
Relative paleointensity
Age (ka)
C)
Age (ka)
Depth (m)
Sed rate (cm/ka)

Fig. 7

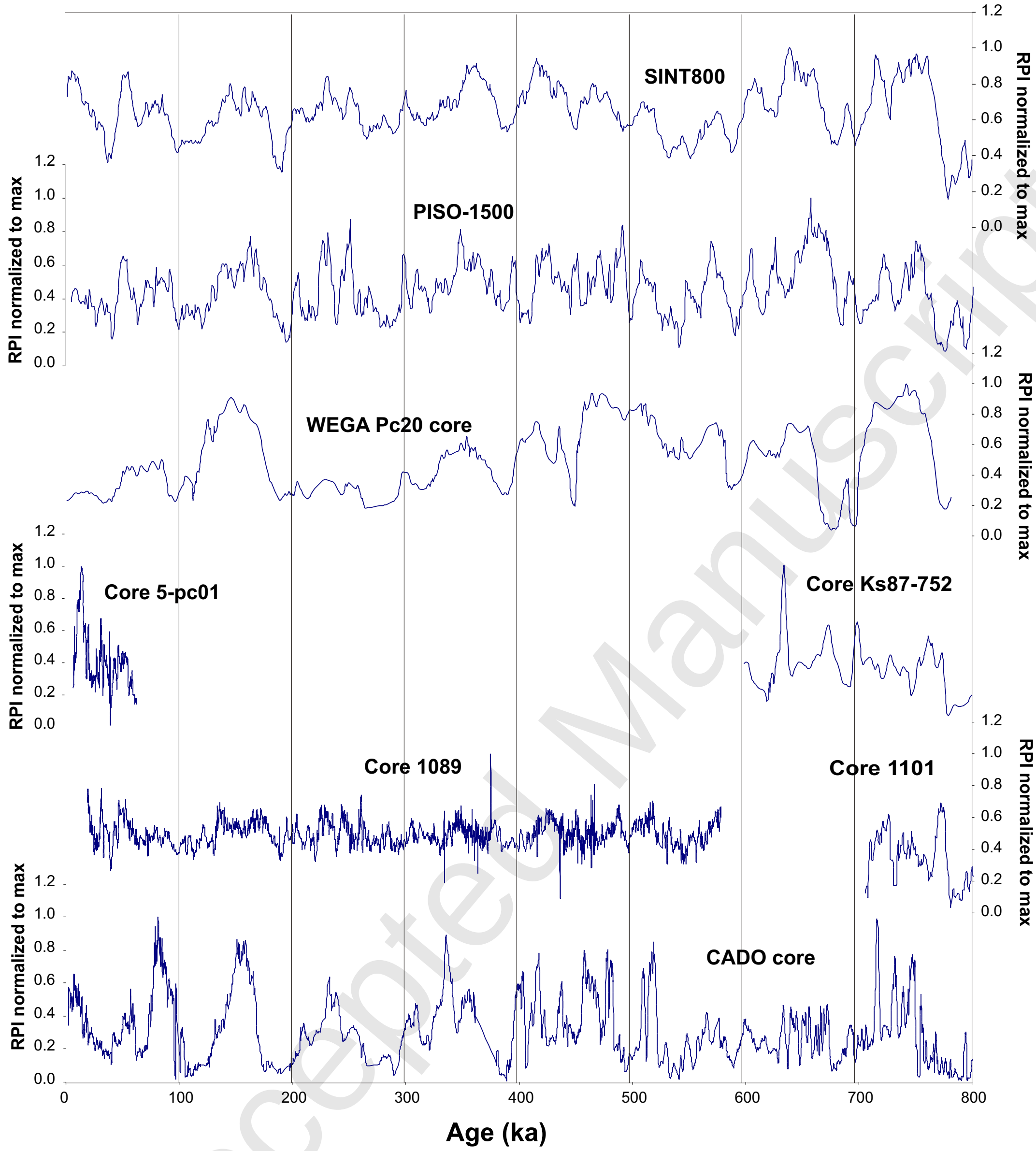
SINT800
PISO-1500
WEGA Pc20 core
Core 5-pc01
Core Ks87-752
Core 1089
Core 1101
CADO core
RPI normalized to max
Age (ka)

Fig. 8

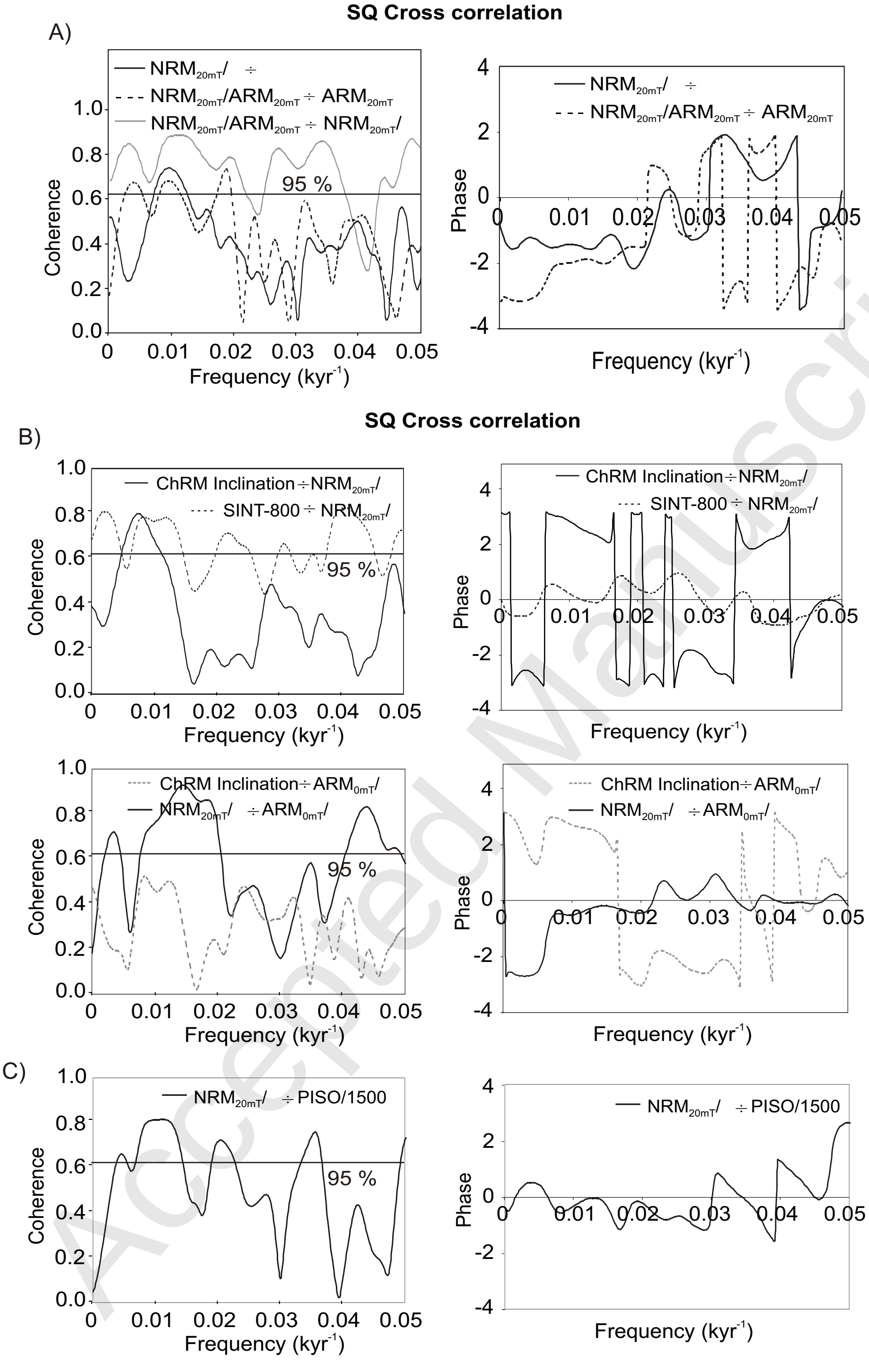

SQ Cross correlation
A)
NRM20mT/ ÷
NRM20mT/ARM20mT ÷ ARM20mT
NRM20mT/ARM20mT ÷ NRM20mT/
95 %
Coherence
Frequency (kyr-1)
Phase
B)
ChRM Inclination÷NRM20mT/
SINT-800 ÷ NRM20mT/
ChRM Inclination÷ARM0mT/
NRM20mT/ ÷ARM0mT/
C)
NRM20mT/ ÷PISO/1500

Fig.9

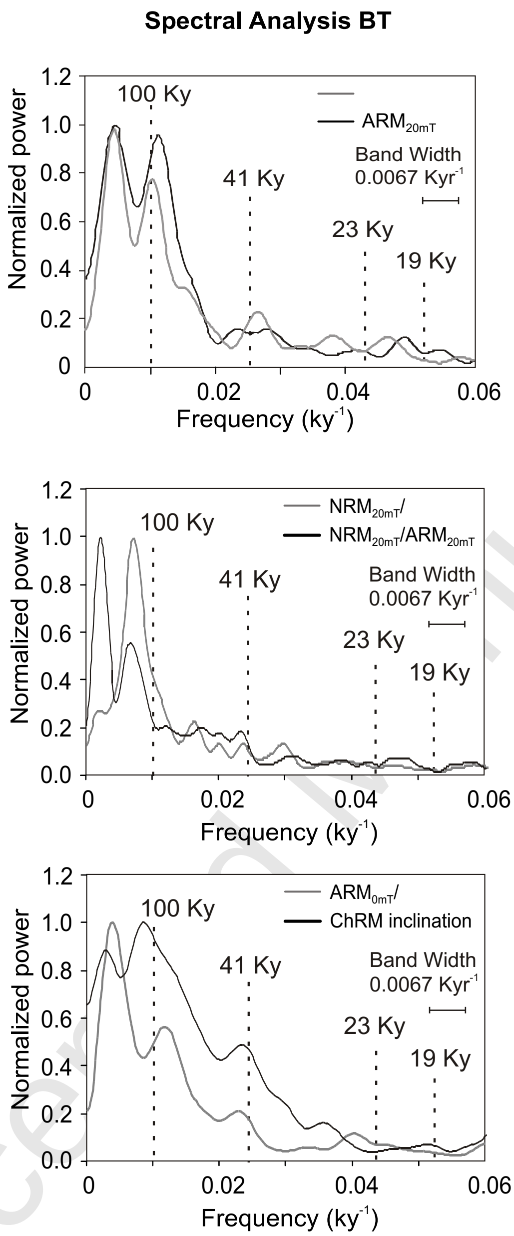
Spectral Analysis BT
100 Ky
ARM20mT
Band Width
0.0067 Kyr-1
41 Ky
23 Ky
19 Ky
Normalized power
Frequency (ky-1)
0
0.02
0.04
0.06
1.2
1.0
0.8
0.6
0.4
0.2
0
NRM20mT/
NRM20mT/ARM20mT
0.0
ARM0mT/
ChRM inclination

Fig. 10

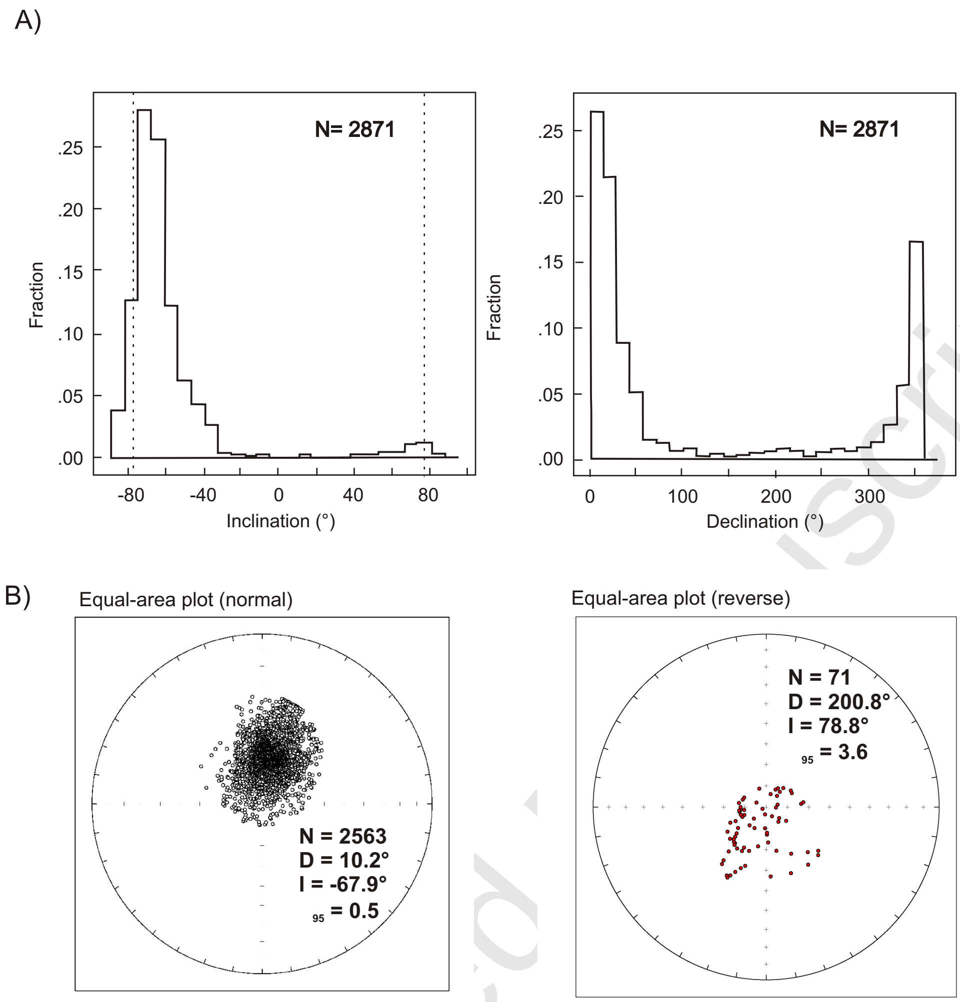

A)
N= 2871
Fraction
.25
.20
.15
.10
.05
.00
-80
-40
0
40
80
Inclination (°)
N= 2871
Fraction
.25
.20
.15
.10
.05
.00
0
100
200
300
Declination (°)
B)
Equal-area plot (normal)
N = 2563
D = 10.2°
I = -67.9°
95 = 0.5
Equal-area plot (reverse)
N = 71
D = 200.8°
I = 78.8°
95 = 3.6

Fig.11

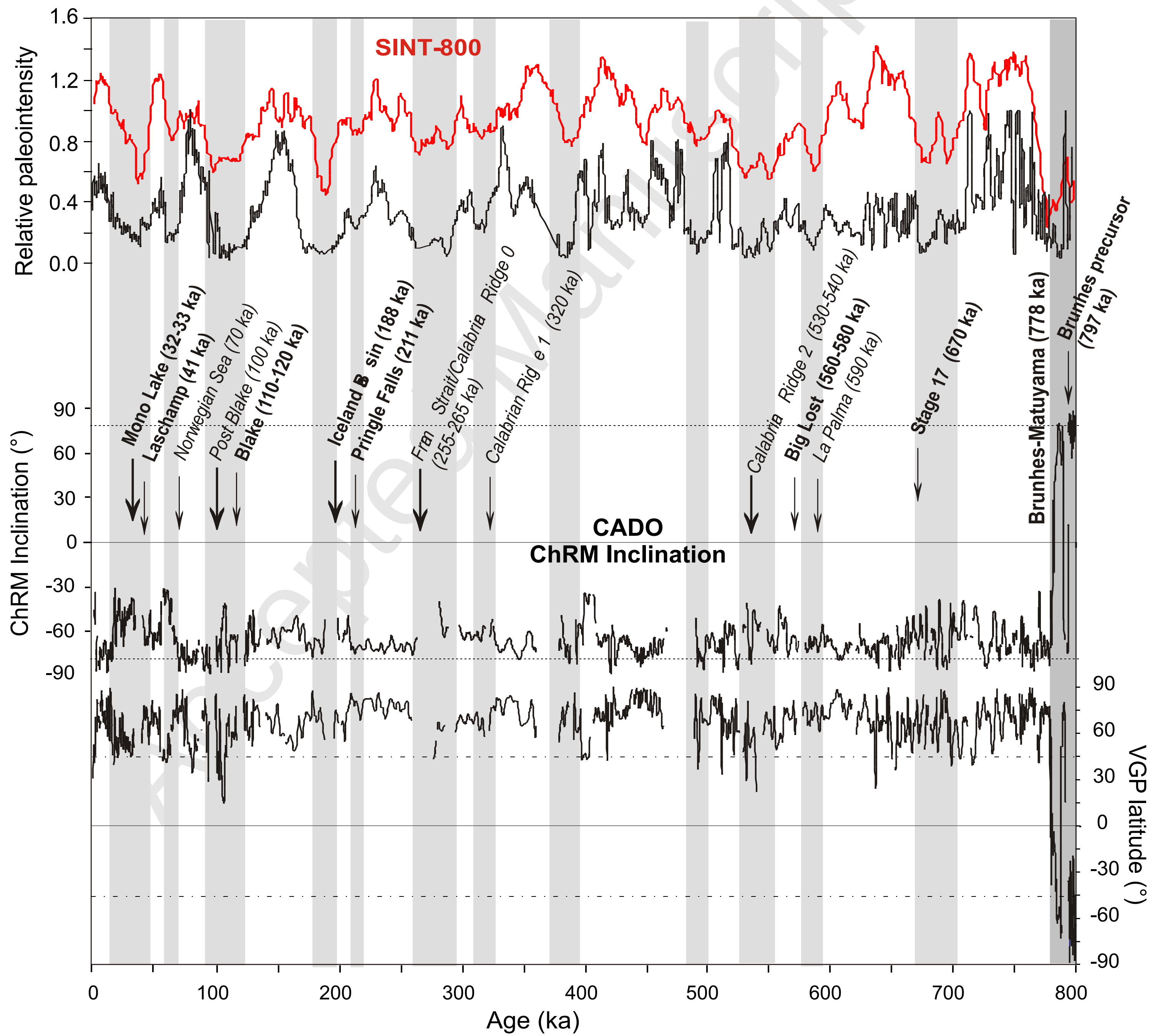
SINT-800
Relative paleointensity
CADO
ChRM Inclination
ChRM Inclination (°)
VGP latitude (°)
Age (ka)
Mono Lake (32-33 ka)
Laschamp (41 ka)
Norwegian Sea (70 ka)
Post Blake (100 ka)
Blake (110-120 ka)
Iceland Basin (188 ka)
Pringle Falls (211 ka)
Fram Strait/Calabria Ridge 0 (255-265 ka)
Calabrian Ridge 1 (320 ka)
Calabria Ridge 2 (530-540 ka)
Big Lost (560-580 ka)
La Palma (590 ka)
Stage 17 (670 ka)
Brunhes-Matuyama (778 ka)
Brunhes precursor (797 ka)

Fig. 12

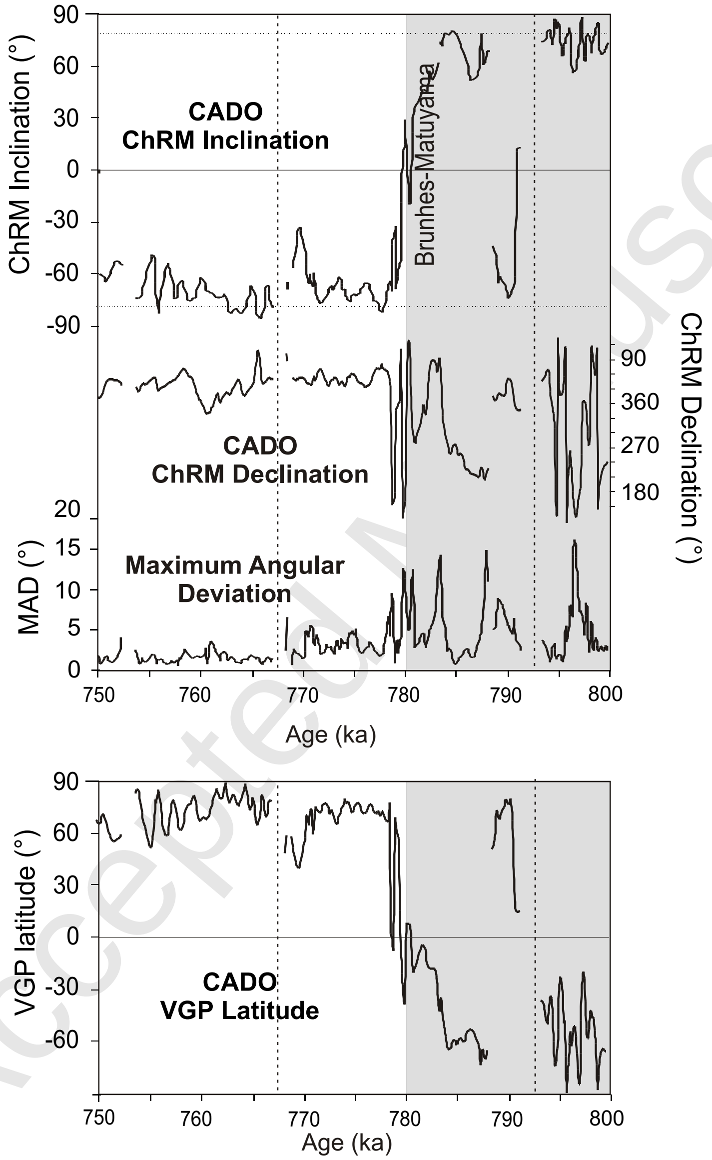
CADO
ChRM Inclination
ChRM Inclination (°)
90
60
30
0
-30
-60
-90
Brunhes-Matuyama
CADO
ChRM Declination
ChRM Declination (°)
90
360
270
180
MAD (°)
20
15
10
5
0
Maximum Angular Deviation
750
760
770
780
790
800
Age (ka)
CADO
VGP Latitude
VGP latitude (°)
90
60
30
0
-30
-60
750
760
770
780
790
800
Age (ka)

Fig.13